Cell

Virus Infection Induces NF-κB-Dependent Interchromosomal Associations Mediating Monoallelic *IFN-β* Gene Expression

Effie Apostolou[1] and Dimitris Thanos[1,*]
[1]Institute of Molecular Biology, Genetics and Biotechnology, Biomedical Research Foundation, Academy of Athens, 4 Soranou Efesiou Street, Athens 11527, Greece
*Correspondence: thanos@bioacademy.gr
DOI 10.1016/j.cell.2008.05.052

SUMMARY

Transcriptional activation of the *IFN-β* gene by virus infection requires the cooperative assembly of an enhanceosome. We report that the stochastic and monoallelic expression of the IFN-β gene depends on interchromosomal associations with three identified distinct genetic loci that could mediate binding of the limiting transcription factor NF-κB to the *IFN-β* enhancer, thus triggering enhanceosome assembly and activation of transcription from this allele. The probability of a cell to express IFN-β is dramatically increased when the cell is transfected with any of these loci. The secreted IFN-β protein induces high-level expression of the enhanceosome factor IRF-7, which in turn promotes enhanceosome assembly and *IFN-β* transcription from the remaining alleles and in other initially nonexpressing cells. Thus, the *IFN-β* enhancer functions in a nonlinear fashion by working as a signal amplifier.

INTRODUCTION

The human antiviral response is triggered by the transcriptional activation of type I interferon genes (20 *IFN-α*, 5 *IFN-ω*, and 1 *IFN-β*) (Paun and Pitha, 2007; Taniguchi and Takaoka, 2002). This leads to the production and secretion of IFN proteins that bind to type I IFN receptors on the surface of both infected and uninfected cells, leading to the expression of a large number of antiviral genes (Stetson and Medzhitov, 2006). Transcriptional activation of the human *IFN-β* gene requires an enhancer element located immediately upstream of the core promoter. The *IFN-β* enhancer is recognized by three distinct sets of transcription factors (NF-κB, IRFs, and ATF-2/cJun) and by the architectural protein HMGI(Y). Virus infection leads to the coordinate activation of all three types of transcription factors, which assemble on the IFN enhancer to form a multiprotein complex known as the *IFN-β* enhanceosome (Thanos and Maniatis, 1995). Enhanceosome assembly occurs only after viral infection and not in response to other signals that can separately activate each of the transcription factors (Thanos and Maniatis, 1995; Lomvardas and Thanos, 2002). This combinatorial mechanism is based on the fact that virus infection is the only known signal that can activate all of the *IFN-β* transcriptional activators simultaneously (Maniatis et al., 1998; Munshi et al., 1999). Following its assembly on the nucleosome-free enhancer, the enhanceosome instructs the ordered recruitment of chromatin modifiers and basal transcription factors to the nearby promoter (Agalioti et al., 2000). This recruitment program culminates with sliding of a nucleosome masking the core promoter, thus allowing the binding of RNA polymerase II and the initiation of transcription (Lomvardas and Thanos, 2001).

The cooperative assembly of the enhanceosome and the organization of nucleosomes in the enhancer/promoter region ensure a high degree of specificity in the transcriptional response. Thus, aberrant transcription from individual transcription factors that are each activated by a variety of other signals (TNF-α, IFNs, stress, etc.) is prevented (Lomvardas and Thanos, 2002). Previous biochemical and structure determination experiments revealed an unexpected complexity in the mechanisms driving enhanceosome assembly. Chromatin immunoprecipitation experiments revealed a stepwise assembly of the enhanceosome (Munshi et al., 2001; Lomvardas and Thanos, 2002). More specifically, NF-κB is initially detected at the IFN-β enhancer at 2 hr after virus infection together with IRF-1, whereas ATF-2 is recruited to the enhancer an hour later followed by the arrival of IRF-3 and c-Jun. IRF-7 is incorporated into the enhanceosome just before initiation of transcription (5–6 hr post-infection). The enhanceosome remains intact for 6 additional hours, and this correlates with the peak of transcriptional activation.

The three-dimensional structure of the intact enhanceosome, as deduced from the assembly of separate structures of pairs of transcription factors bound to their sites, revealed that cooperative assembly derives from binding-induced changes in DNA conformation and to a lesser extent from protein-protein interactions (Escalante et al., 2007; Panne et al., 2007). This observation is in agreement with the stepwise assembly of the enhanceosome in vivo (Munshi et al., 2001), during which the sequential arrival of transcription factors onto the enhancer alters the DNA structure, thus allowing the subsequent binding of the nearby factors.

A striking feature of *IFN-β* expression (Zawatzky et al., 1985; Enoch et al., 1986; Senger et al., 2000; Hu et al., 2007), as well as of many other cytokine genes, including *IL-2* (Holländer et al., 1998), *IL-4* (Riviere et al., 1998), *IL-5* (Kelly and Locksley,

2000), *IL-13* (Kelly et Locksley, 2000; Guo et al., 2005), and *IL-10* (Calado et al., 2006), is that, even under optimal conditions, only a fraction of the cells in the population expresses the cytokine gene at any given moment. This heterogeneity is not due to mixed populations of producing and nonproducing cells but rather is a stochastic phenomenon, as revealed by cell cloning experiments (Zawatzky et al., 1985). An additional characteristic of cytokine gene expression is that gene activation is predominantly monoallelic, thus further underscoring the stochastic mode of gene regulation. A recent study applying single cell RT-PCR analysis and stochastic model simulation provided initial evidence for allelic imbalance of virus-induced *IFN-β* gene transcription (Hu et al., 2007). However, the mechanisms of stochastic *IFN-β* gene expression and allelic imbalance remain elusive.

What transcription mechanism can assure the random choice of cells expressing IFN-β after virus infection? One attractive model invokes the transcription process itself and therefore is likely associated with the inherent complexity of enhanceosome assembly on the *IFN-β* enhancer/promoter. Since enhanceosome assembly is a cooperative process, we asked whether limiting concentrations of one or some of the *IFN-β* activators accounts for the stochastic assembly of enhanceosomes thus leading to binary transcriptional switches. We present evidence for a model in which virus infection induces the stochastic expression of the *IFN-β* gene from a single allele in a small population of cells. The choice of the allele to be expressed depends on interchromosomal associations with three identified distinct genetic loci that could mediate binding of the limiting transcription factor NF-κB to the *IFN-β* enhancer promoting enhanceosome assembly and activation of transcription from this allele. The secreted IFN-β protein induces high-level expression of the enhanceosome factor IRF-7, which in turn promotes enhanceosome assembly and *IFN-β* transcription from the remaining alleles and in other initially nonexpressing cells. Thus, the *IFN-β* enhancer functions in a nonlinear fashion and works as a signal amplifier.

RESULTS

Limiting Amounts of NF-κB and IRF Proteins Contribute to the Stochastic Expression of the *IFN-β* Gene

To investigate whether individual enhanceosome components are present in cells at suboptimal concentrations, we transfected HeLa cells with expression vectors producing each of the *IFN-β* activators, followed by virus infection for 6 hr and hybridization with an antisense *IFN-β* digoxigenin-labeled RNA probe. Control experiments using GFP reporters have indicated that under our conditions approximately 90% of HeLa cells can be transfected (data not shown). Figures 1A and 1B show that only 20% of the cells in the population transcribe the *IFN-β* gene in response to virus infection, a result consistent with previous studies (Zawatzky et al., 1985; Enoch et al., 1986; Senger et al., 2000; Hu et al., 2007). Remarkably, the percentage of IFN-β-producing cells after virus infection increases to 75%, when the cells were transfected with an expression vector producing the p65 subunit of NF-κB and to 55% after IRF-7 expression. Smaller increases were observed when either ATF-2/cJun, IRF-1, or IRF-3 were expressed, whereas increasing the concentration of HMGI(Y) did not affect the number of cells expressing IFN-β (Figures 1A and 1B). In control experiments we showed that hybridization with a sense *IFN-β* RNA probe did not produce a signal (data not shown). The increase in the number of IFN-β-producing cells is also reflected in the amount of total *IFN-β* mRNA produced, as seen by the RT-PCR experiment shown in Figure 1C. These experiments suggest that NF-κB, IRF-7, IRF-3, and to a lesser extent ATF-2/cJun and IRF-1 exist at suboptimal concentrations within the cells and the failure of some cells to express IFN-β can be bypassed by increasing the cellular concentration of these proteins. The increase of IFN-β-expressing cells is not observed in uninfected cells (not shown), indicating that overexpression of these factors did not bypass the requirement for enhanceosome assembly after virus infection. To test whether NF-κB overexpression increases not only the percentage of IFN-β-expressing cells but also the amount of *IFN-β* mRNA produced per cell, we carried out the experiment shown in Figure 1D. HeLa cells were transfected with the NF-κB expression vector along with a GFP vector and the cells were either mock or virus infected. GFP-positive cells were isolated by cell sorting, and the amount of *IFN-β* mRNA was determined by real-time RT-PCR. As seen in the figure, the increase in *IFN-β* mRNA production (4.1-fold) is similar to the increase of the number of cells (3.5-fold) producing *IFN-β* expression following NF-κB overexpression (Figure 1B). Thus, the *IFN-β* expression levels per cell are not significantly affected by NF-κB overexpression.

Virus Infection Induces Colocalization of the *IFN-β* Gene with Three Distant NF-κB Bound Genomic Loci

The low concentration of NF-κB within cells (approximately 50.000 molecules, Hottiger et al., 1998; Lipniacki et al., 2006; and our unpublished data) when taken together with the fact that it is the first factor that binds to the *IFN-β* promoter (Munshi et al., 2001) poses a major question regarding the mechanism by which NF-κB locates the *IFN-β* gene and nucleates enhanceosome assembly in the context of the human genome. We hypothesized that there exist "specialized" NF-κB sites that might be capable of interacting with NF-κB immediately and preferentially after its entry into the nucleus. Next, NF-κB could associate with the promoters of target genes via inter- and/or intrachromosomal interactions, thus "delivering" the factor to the correct site. Since interchromosomal interactions are stochastic in nature (de Laat and Grosveld, 2007; Misteli 2007), such a model could explain some of the features of *IFN-β* expression discussed above. To test this idea we employed circular chromosome conformation capture (4C) (Ling et al., 2006; Zhao et al., 2006) coupled with chromatin immunoprecipitation (Figure 2A). The 4C method is based on the proximity ligation principle, in which DNA-protein complexes existing in *trans* will generate circular DNA molecules (3C) (Dekker et al., 2002). Sequences interacting with a known gene (*IFN-β*) can be cloned by inverse PCR using gene-specific primers without any prior knowledge of their identities. HeLa cells were mock or virus infected for 4 hr, followed by formaldehyde crosslinking. The crosslinked chromatin was digested with EcoRI (flanking the *IFN-β* gene), followed by chromatin immunoprecipitation using a p65-specific antibody. The

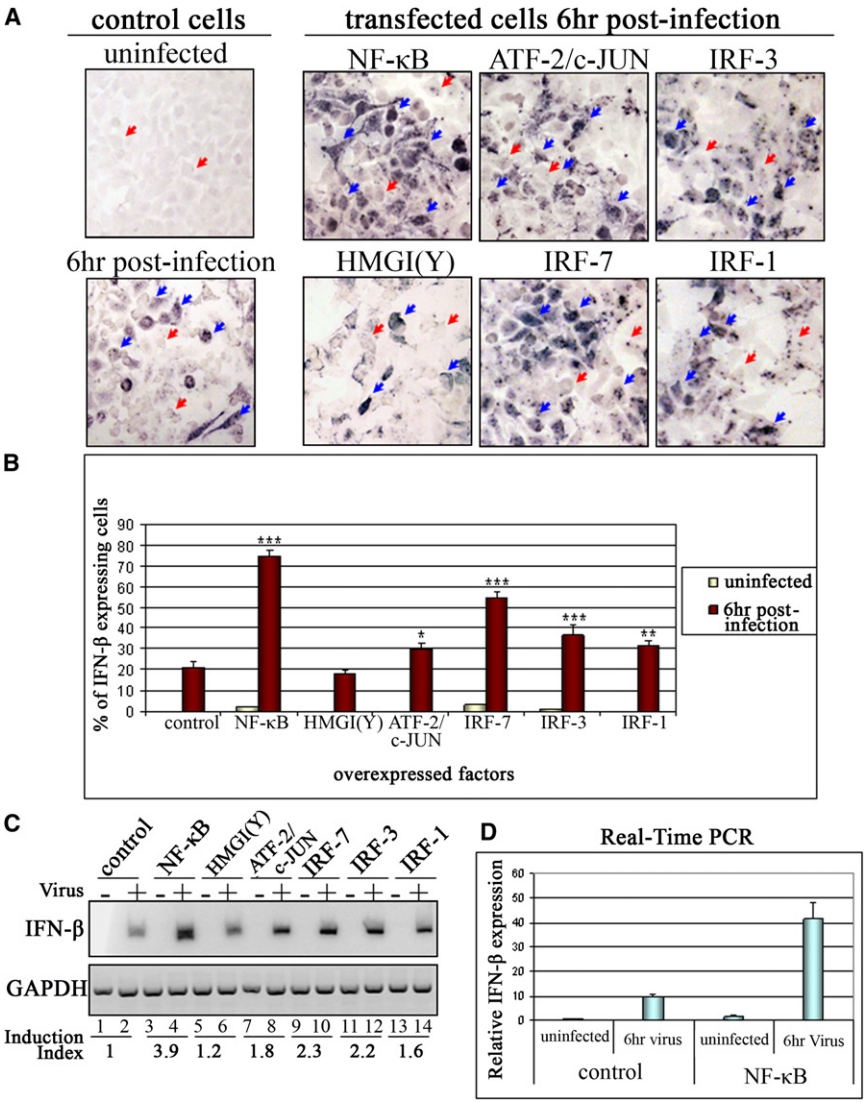

Figure 1. NF-κB Is the Most Limiting Factor Required for *IFN-β* Enhanceosome Assembly In Vivo

(A) HeLa cells were transfected with empty or expression vectors encoding each of the *IFN-β* gene activators. Six hours post-infection the cells were fixed and IFN-β expression in individual cells was detected by in situ hybridization using an antisense RNA *IFN-β* probe labeled with digoxygenin ribonucleotides followed by incubation with an anti-DIG antibody conjugated with alkaline phosphatase. The top left panel shows uninfected cells. The red and blue arrows indicate representative nonexpressing and expressing cells, respectively.

(B) Diagrammatic representation of the percentage (mean ± standard deviation [SD]) of cells expressing IFN-β from three independent in situ hybridization experiments performed as in (A). All cells for each category were scored blindly, and at least 300 cells were counted in each case. * denotes $p < 0.05$, ** denotes $p < 0.01$, and *** denotes $p < 0.001$.

(C) RT-PCR analysis illustrating IFN-β expression in HeLa cells transfected with the indicated *IFN-β* transcriptional regulators. The bottom part of the figure shows the induction index derived by quantitating three independent experiments.

(D) HeLa cells were transfected with the p65 expression vector along with a GFP-expressing plasmid followed by mock or virus infection. GFP-positive cells were isolated by cell sorting and the abundance of *IFN-β* mRNA was determined by real-time RT-PCR analysis (shown are mean values ± SD).

precipitated and digested chromatin was diluted and DNA ligase was added to covalently link DNA sequences that colocalize in the nucleus independent of their location. After removing the protein, nested PCR primers were used to detect interacting sequences. Using a pair of nested PCR primers (Figure 2A) we detected sequences from a wide range of sizes in the crosslinked chromatin (Figure 2B, lane 4) derived from virus-infected cells but not in any of the controls, including genomic DNA (Figure 2B, lane 1), EcoRI-cleaved but not ligated chromatin DNA (lane 2) derived from virus-infected cells, or EcoRI-cleaved and -ligated chromatin DNA derived from uninfected cells (lane 3). Subsequent sequence analysis of the 4C samples from virus-infected cells identified three unique sequences that appear to interact with *IFN-β* (Figures 2C and S1 available online). Remarkably, all three clones possess specialized Alu repeats, known as AluSX and AluY (Polak and Domany, 2006), which contain the putative NF-κB binding site GGGTTTCACC deviating from the consensus GGGRNYYCC in two nucleotides (underlined). Clones #14 and #9 contain two copies of the specialized NF-κB motif (Figure S1). Clone #21 resides on chromosome 4, #14 on chromosome 9, and #9 on chromosome 18. Of note, the *IFN-β* gene resides on chromosome 9 (9p21). Thus, #14 and *IFN-β* reside near the two ends of chromosome 9 in humans.

To examine whether the three identified loci interact with the *IFN-β* locus, we performed 3C assays using primers specific for *IFN-β* and for each of the clones. Figure 2D (lanes 1, 7, and 13) shows that in uninfected cells there is no detectable PCR product generated using primer pairs either from #21, or #14, or #9 and *IFN-β*. However, PCR products were detected when the chromatin DNA used was prepared from virus-infected cells (Figure 2D, lanes 2–4, 8–10, and 14–16). The products were detected as early as 2 hr after virus infection, peaked at 4 hr, and were decreased at 6 hr post-infection, indicating that these interactions occur primarily during enhanceosome assembly at the *IFN-β* locus. In each instance, the size of the PCR products was that predicted for the ligation of *IFN-β* with each of the clones and the identity of the products was confirmed by DNA sequence analysis (data not shown). Furthermore, the specificity of the interactions between the *IFN-β* locus and at least one of

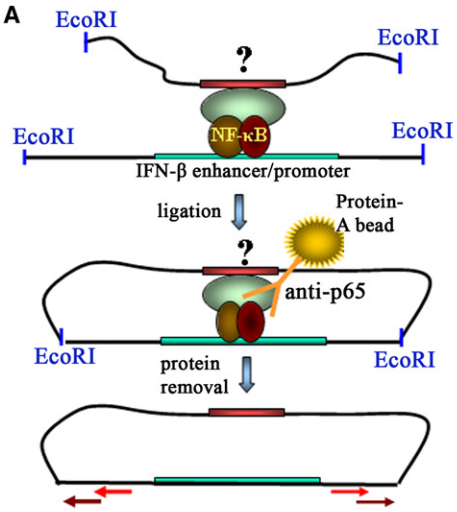

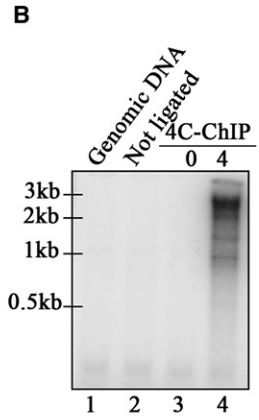

C

4C-ChIP clone number	Precise position	Nearby genes	Alu element
#21	4p13	19kb upstream of **RHOH** 20kb downstream of **N4BP2**	AluSX (GGGTTTCACC)
#14	9q33	10kb upsteram of **ABO** 15kb downstream of **LCN1**	AluY (GGGTTTCACC)
#9	18q21	12kb upstream of **LOXHD1**	AluSX (GGGTTTCACC)

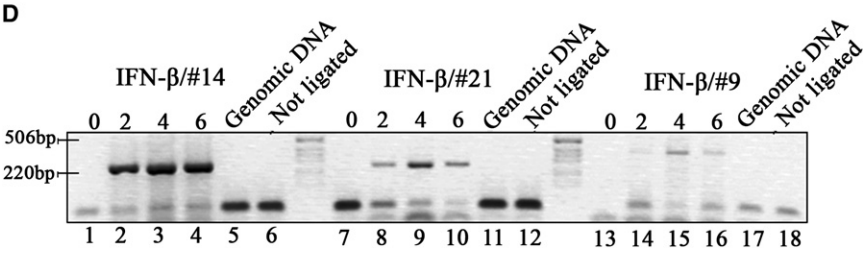

Figure 2. Identification of *IFN-β* Locus-Interacting Genomic Regions using 4C-ChIP

(A) Schematic representation of the 4C-ChIP assay. The EcoRI fragment bearing the *IFN-β* promoter is shown in green whereas EcoRI fragments bearing putative interacting loci are shown in red. The transcription factor NF-κB is shown bound on the *IFN-β* enhancer. The red arrows indicate nested primers designed near the EcoRI sites flanking the *IFN-β* locus.

(B) Shown is an agarose gel depicting nested inverse polymerase chain reactions of 4C-ChIP samples. After amplification only crosslinked, digested, and ligated chromatin DNA derived from virus-infected cells generated amplified sequences of different sizes.

(C) Short description of 4C-ChIP clones.

(D) Agarose gel electrophoresis of the PCR products using nested primers specific to the *IFN-β* locus together with primers specific for the 4C-ChIP clones #14, #21, and #9. PCR was performed on EcoRI-digested chromatin derived from HeLa cells mock- or virus-infected for 2, 4, and 6 hr. Genomic DNA and crosslinked digested but not ligated chromatin derived from 4 hr infected cells were used as controls. Size markers were loaded between lanes 6 and 7, 12 and 13.

the clones (#21) was verified in 4C-ChIP experiments using inverse PCR-nested primers from the genomic locus of #21. In this experiment we cloned the *IFN-β* locus three times, underscoring the strength and the specificity of these interactions (data not shown).

To further validate the 4C data and to demonstrate the physical colocalization of IFN-β with clones #21, #9, and #14, we performed three-dimensional DNA fluorescence in situ hybridization (FISH) analysis using HeLa cells that were either mock or virus infected for 4 hr. Figure 3A shows that the *IFN-β* probe detects six or seven *IFN-β* genes, whereas probes for #21, #9, and #14 detect three, three, and six or seven loci in HeLa cells, respectively. This is due to the fact that HeLa cells are polyploid. In mock-infected cells we detected no evidence of colocalization between *IFN-β* and any of the clones (Figure 3A, left column). Remarkably, in some virus-infected cells, one allele of *IFN-β* is specifically colocalized with one allele of #21, or #14, or #9 (Figure 3, right column). FISH experiments using a BAC clone containing different AluSX repeats fail to detect colocalization with the *IFN-β* locus before or after virus infection (not shown). These FISH experiments confirmed our results obtained using the 3C technique (Figure 2). FISH experiments performed on nuclei from virus-infected cells for different amounts of time indicated that these interactions are transient since they appear 2 hr post-infection, peak at 4 hr, and decline significantly at 8 hr post-infection (Figure 3B), a result consistent with the 3C analysis of Figure 2D. Thus, interchromosomal associations between the *IFN-β* locus and these loci occur at maximal frequencies before initiation of transcription and during enhanceosome assembly (2–6 hr), and they are significantly reduced at the time of initiation and propagation of transcription (6–8 hr).

In control experiments, FISH was performed with the *IL-8* gene (a known NF-κB target virus-inducible gene) and clones #21, #14, and #9 in mock- or virus-infected cells. No specific colocalization was detected between these loci and the *IL-8* gene, nor between the *IFN-β* and *IL-8* genes (data not shown). By contrast, the 4C clone #21 (#14 and #9 not shown) was colocalized with the *IκBα* gene (another NF-κB target) (Figure S2). The interaction between *IκBα* and our 4C clones prompted us to examine whether the *IFN-β* and *IκBα* genes are colocalized after virus infection. As seen in Figure S2, 11% of virus-infected cells show colocalization between the *IFN-β* and *IκBα* genes. Thus, the *IFN-β* and *IκBα* genes, which are activated by NF-κB, colocalize after virus infection. These colocalizations appear to be gene specific since not all NF-κB-regulated genes colocalize either with the 4C clones or between them.

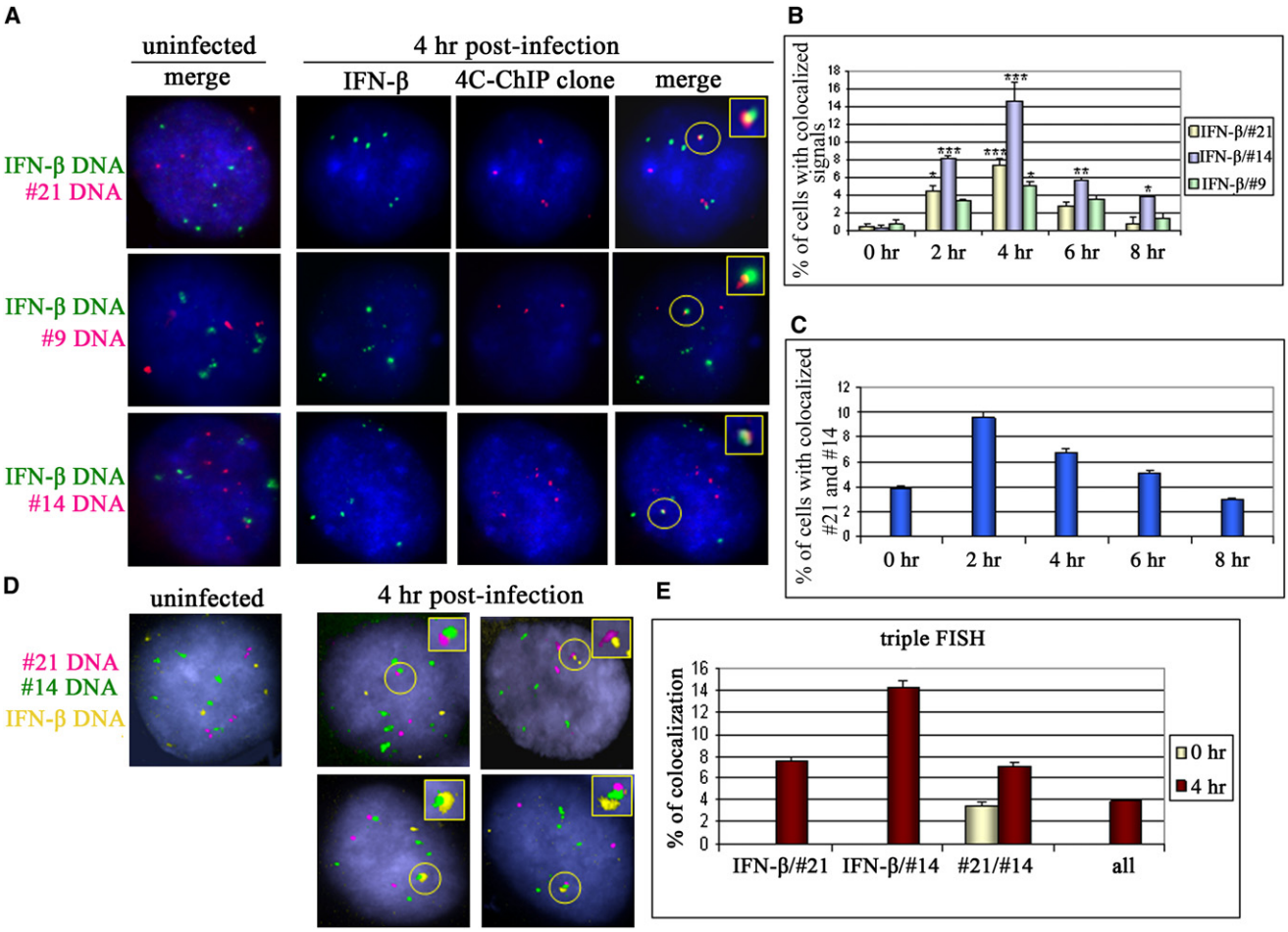

Figure 3. DNA FISH Reveals the Colocalization of the *IFN-β* Locus and the 4C-ChIP Clones following Virus Infection

(A) A digoxygenin-labeled DNA probe was used to detect the *IFN-β* locus and was visualized with FITC-conjugated anti-DIG antibody (green). A biotin-labeled DNA probe was used to detect the 4C-ChIP clones, as indicated in the figure, and was visualized with Alexa 568-conjugated streptavidin (red). The circle includes the colocalized alleles observed only in virus-infected cells. A magnification of the area of colocalization is shown at the top right.

(B) Diagrammatic representation of the percentage (mean ± SD) of cells with colocalization between *IFN-β* and each of the 4C-ChIP clones during the time course of virus infection. All cells were scored blindly and slides were prepared from three different experiments. Scores were derived from 250 to 486 cells for each category. * denotes $p < 0.05$, ** denotes $p < 0.01$, and *** denotes $p < 0.001$.

(C) Diagrammatic representation of DNA FISH experiments showing the percentage (mean ± SD) of cells with colocalized signals of #21 and #14 in the time course of virus infection. Of note, relatively high frequency of colocalization is observed in uninfected cells.

(D) Triple DNA FISH experiment revealed the simultaneous colocalization of *IFN-β* with #21 and #14 upon virus infection. The *IFN-β* locus was detected with far red (yellow).

(E) Diagrammatic representation of triple DNA FISH experiments showing the percentage (mean ± SD) of cells with colocalized signals of each combination of the indicated genomic loci.

To test whether the 4C isolated genomic loci colocalize before or after virus infection, we carried out FISH experiments using probes for each 4C clone. The results showed a markedly high frequency of colocalization between 4C clones #14 and #21 even before virus infection (Figure 3C). These interactions are specific since the *IFN-β* gene located on the same chromosome as #14 does not colocalize with any of these clones before virus infection. The interchromosomal interactions are further increased upon virus infection (Figure 3C). Remarkably, triple FISH experiments revealed the simultaneous interaction of *IFN-β* with these 4C loci, albeit in a lower percentage of cells (Figures 3D and 3E). These results showed that the widely separated 4C clones colocalize before virus infection and interact together with the *IFN-β* gene after virus infection.

4C Clones Colocalize with Monoallelically Expressed *IFN-β* RNA

We have shown that one *IFN-β* allele interacts with one allele from each of the 4C clones only in response to virus infection (Figure 3). At the peak of interaction (Figure 3B), the total percentage of *IFN-β* interacting alleles in the cell population is 27%, a number that is similar to the percentage of cells expressing IFN-β following virus infection (Figure 1). Therefore, we asked whether these interchromosomal interactions correlate with

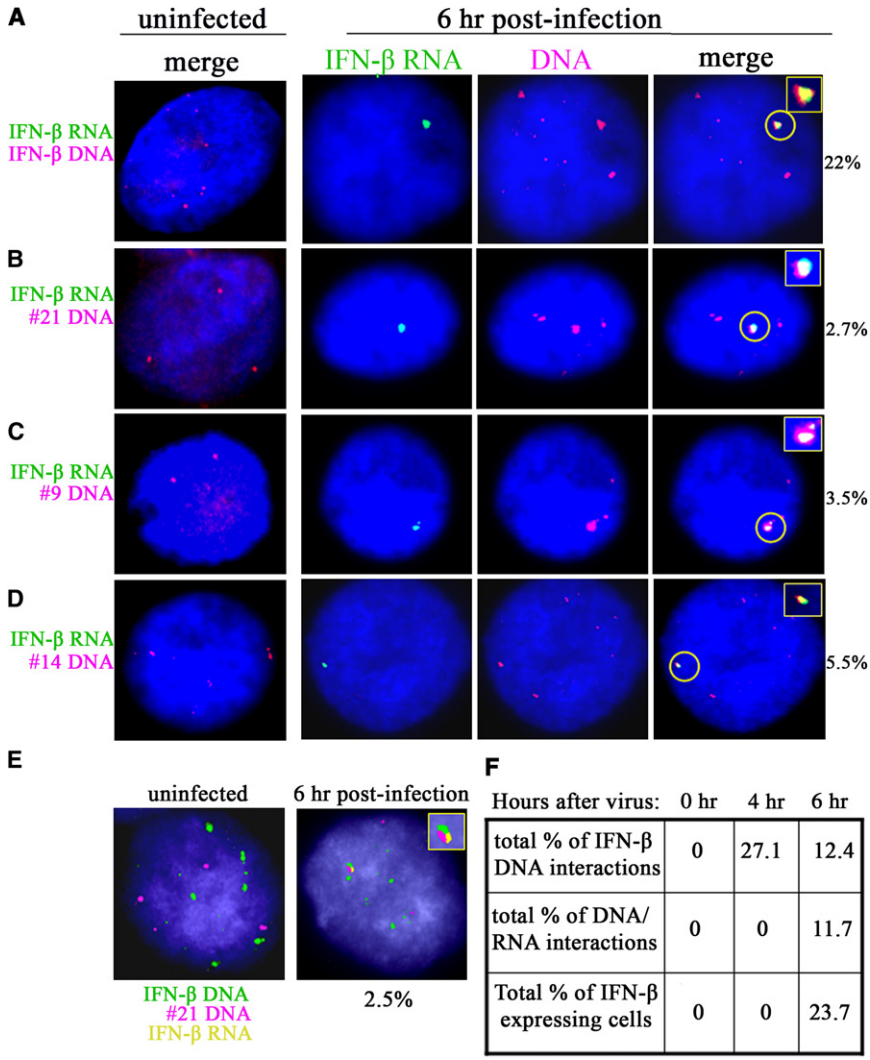

Figure 4. RNA and DNA FISH on Virus-Infected Cells Reveal Colocalization of the 4C-ChIP Clones with the Transcriptionally Active *IFN-β* Allele

(A) Combined RNA and DNA FISH on nuclei from mock- and virus-infected for 6 hr HeLa cells. DIG-labeled nick-translated *IFN-β* probe was used for the detection of the *IFN-β* nuclear transcripts. The signal was visualized with FITC-conjugated anti-DIG antibody (green). A biotin-labeled DNA probe was used for the detection of the *IFN-β* locus and was visualized with Alexa 568-conjugated streptavidin (red). The nuclei were counterstained with DAPI (blue). RNA FISH detects the virus-inducible single transcriptionally active *IFN-β* allele, whereas DNA FISH detects all 6 *IFN-β* alleles in HeLa cells. The percentage of expressing cells is shown on the right.

(B) RNA FISH to detect *IFN-β* nuclear RNA (green) combined with DNA FISH detecting the #21 locus (red). The transcriptionally active *IFN-β* allele colocalizes with a single #21 allele at a frequency indicated at the right.

(C) RNA FISH to detect *IFN-β* nuclear RNA (green) combined with DNA FISH detecting the #9 locus (red). The transcriptionally active *IFN-β* allele colocalizes with a single #9 allele at a frequency indicated at the right.

(D) RNA FISH to detect IFN-β nuclear RNA (green) combined with DNA FISH detecting the #14 locus (red). The transcriptionally active *IFN-β* allele colocalizes with a single #14 allele at a frequency indicated at the right.

(E) Triple RNA/DNA FISH experiment revealed the simultaneous colocalization of the *IFN-β* gene (green) with #21 (red) and *IFN-β* mRNA (yellow) upon virus infection.

(F) Frequency of colocalization of *IFN-β* with the 4C clones and its correlation with monoallelic stochastic *IFN-β* expression.

IFN-β RNA production. We combined DNA FISH with RNA FISH to determine whether the 4C clones colocalize with the transcribed *IFN-β* gene following virus infection. Figure 4A shows that only one IFN-β allele is transcribed at 6 hr following virus infection. Remarkably, this allele colocalizes with a single allele from the 4C clones (Figures 4B–4D) with frequencies similar to those described in Figure 3B for the 6 hr time point. The triple RNA/DNA FISH experiment of Figure 4E shows that the single *IFN-β* allele interacting with the 4C clone #21 is the one expressing *IFN-β* mRNA. As a control we showed that the *IFN-β* RNA is not detected in uninfected cells and that the *IFN-β* RNA signal is lost when virus-infected cells are treated with RNase A (data not shown). Taken together, these results suggest that interchromosomal associations occurring between single alleles from the 4C clones and *IFN-β* in a cell population correlate with monoallelic *IFN-β* transcription. The total percentage of cells showing maximal monoallelic interchromosomal interactions at 4 hr post-infection (27.1%, Figure 4F) correlates to the total percentage of cells expressing the *IFN-β* gene from a single allele at 6 hr (22%, Figure 4A). These experiments suggest that the *IFN-β* RNA is transcribed from a single *IFN-β* allele interacting with a single allele from any of the 4C isolated loci.

Since the experiments described above have been carried out in HeLa cells that are polyploid, we repeated the DNA, DNA-RNA FISH, and the triple FISH experiments in diploid human epithelial cells (HCT-116) and obtained qualitatively similar results (Figure S3), thus indicating the biological significance of our observations.

IFN-β Gene Transcription Switches from Monoallelic to Multiallelic in Response to IFN-β Cytokine Signaling

The experiments of Figure 4 were performed using cells infected with virus for 6 hr. This is the time point at which *IFN-β* transcription begins. However, at this time point there is a decreased interaction between *IFN-β* and the 4C clones, and this interaction is lost at the peak of *IFN-β* transcription (Figure 3). Since there are no interchromosomal interactions at later time points (not shown) we can't further correlate *IFN-β* RNA expression with interaction with the 4C clones. However, when we repeated the DNA-RNA FISH using *IFN-β* probes and cells infected with

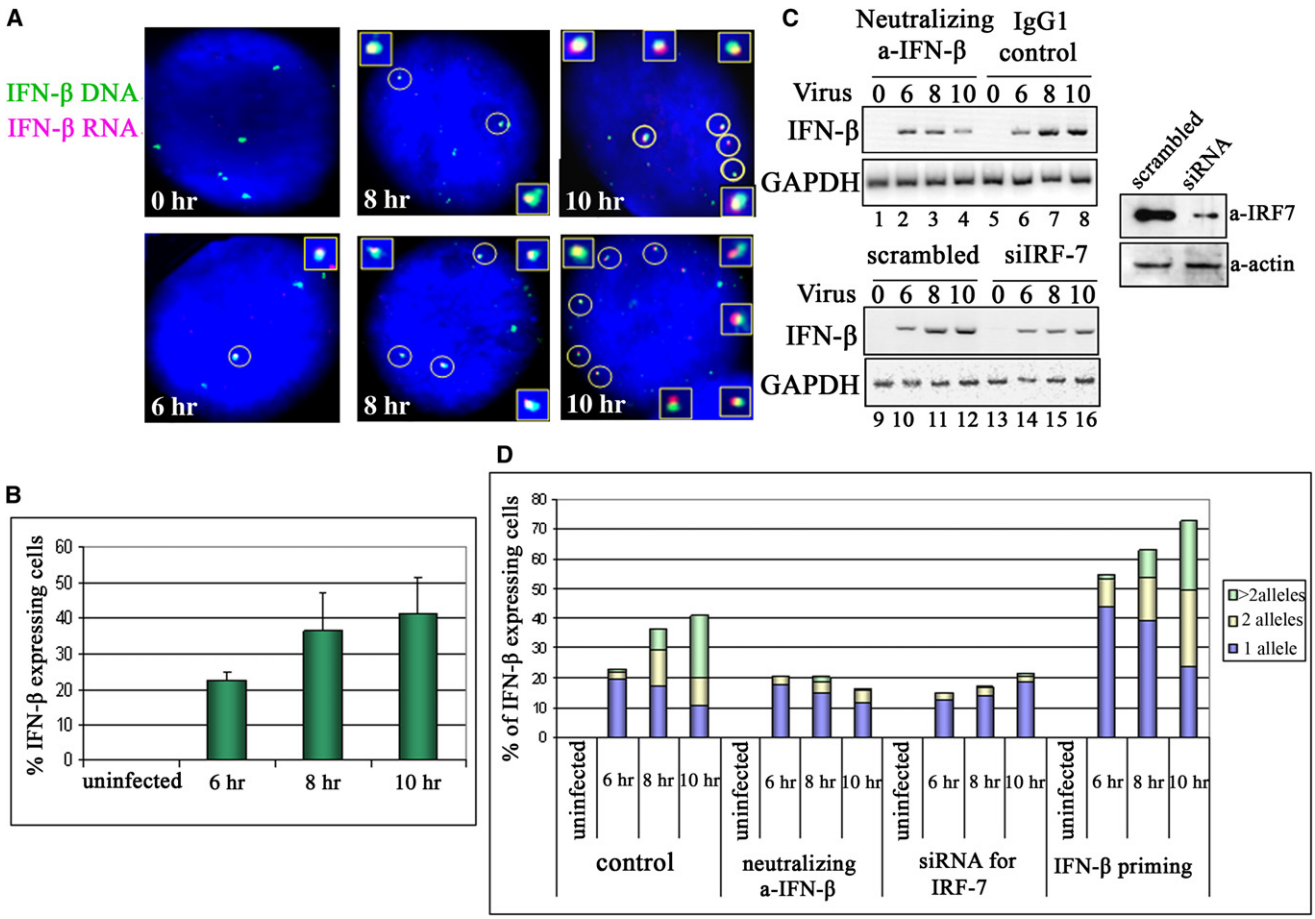

Figure 5. *IFN-β* Gene Transcription Switch from Monoallelic to Multiallelic during the Time Course of Virus Infection Requires IRF-7

(A) Combined RNA and DNA FISH on nuclei from mock- and virus-infected HeLa cells for 6, 8, and 10 hr. Biotin-labeled nick-translated *IFN-β* probe was used for the detection of the *IFN-β* nuclear transcripts. The signal was visualized with Alexa 568-conjugated streptavidin (red). A DIG-labeled DNA probe was used for the detection of the *IFN-β* locus and was visualized with FITC-conjugated anti-DIG antibody (green). The nuclei were counterstained with DAPI (blue). RNA FISH detects a single transcriptionally active *IFN-β* allele at 6 hr post-infection and additional *IFN-β*-expressing alleles at later time points.

(B) Diagrammatic representation of the percentage (mean ± SD) of cells expressing IFN-β from three independent in situ hybridization experiments performed as in Figure 1 except that the cells were infected with virus for 6, 8, or 10 hr. All cells for each category were scored blindly and at least 220 cells were counted in each case.

(C) HeLa cells were mock- or virus-infected for 6, 8, or 10 hr in the presence of IFN-β neutralizing antibodies or IgG1 as a control (lanes 1–8). RNA was isolated and the abundance of the *IFN-β* transcripts was determined by RT-PCR analysis. In the bottom panel (lanes 9–16) the cells were treated with scrambled siRNA or siRNA specific for IRF-7 for 62 hr before virus infection and RT-PCR analysis. The efficiency of the siRNA knockdown was tested by western blot (shown on the right of the figure) using extracts prepared from virus-infected cells.

(D) Diagrammatic representation of the percentage of cells and the number of *IFN-β*-expressing alleles per cell from two independent RNA/DNA FISH experiments performed as in Figure 4 except that the cells were treated as in (C). All cells for each category were scored blindly and at least 130 cells were counted in each case. In each column the relative percentage of cells expressing 1, 2, or more *IFN-β* alleles is indicated with different colors.

Sendai virus for longer times we found that gradually the remaining *IFN-β* alleles begin to express *IFN-β* RNA (Figure 5A), a result consistent with the gradual decrease of intrinsic noise of *IFN-β* expression reported recently (Hu et al., 2007). The in situ hybridization experiment of Figure 5B shows that the percentage of cells expressing IFN-β is nearly doubled at 10 hr post virus infection as opposed to the percentage of expressing cells at 6 hr post-infection. In summary, *IFN-β* transcription begins from a single allele interacting with the 4C clones in 20% of the cells but at later time points the remaining *IFN-β* alleles, not interacting with the 4C clones, begin to express IFN-β in the same and in other cells.

To test whether the IFN-β protein produced early in virus infection from a single allele is critical for the subsequent multiallelic expression (positive feedback) of the same and other cells we added neutralizing IFN-β antibodies in the culture. Figure 5C shows that the neutralizing antibodies dramatically decreased IFN-β expression at 8 and 10 hr post-infection, but they did not affect the early monoallelic activation of the gene (compare lanes 1–4 with 5–8). To determine whether the effect of the IFN-β protein on *IFN-β* gene expression is mediated through IRF-7, which is an IFN-β-inducible factor (Sato et al., 2000), we treated the cells with an IRF-7-specific siRNA. As seen in Figure 5C (lanes 9–16), IRF-7 is critical for maximal *IFN-β* transcription especially

at the later time points, and it has a small effect at the early phase of induction, a result consistent with the late arrival of IRF-7 on the *IFN-β* enhancer (Munshi et al., 2001).

To correlate the IFN-β protein effect on *IFN-β* gene transcription with the switch from mono- to multiallelic expression we carried out DNA and RNA FISH experiments to determine the number of *IFN-β* alleles expressing the *IFN-β* gene. Figure 5D shows that 22% of the cells infected with Sendai virus for 6 hr express IFN-β, and of these the majority (19% of total cells) transcribe the *IFN-β* gene from a single allele. However, at 8 hr post-infection there is a parallel decrease of monoallelic expressing cells and an increase of cells expressing IFN-β from two or more alleles. This switch is more dramatic at 10 hr post-infection when the majority of the expressing cells transcribe the *IFN-β* gene from two or more alleles. Treatment of the cell culture with neutralizing IFN-β antibodies affected monoallelic expression only slightly, but it dramatically reduced both the total number of cells expressing IFN-β at later time points and the switch from mono to multiallelic IFN-β expression. A similar result was obtained when the cells were treated with the IRF-7-specific siRNA (Figure 5D). These experiments demonstrate that the IFN-β protein secreted early on at virus infection is produced from cells transcribing a single *IFN-β* gene allele and acts on the same and on other cells to induce *IFN-β* gene transcription on all alleles. A prediction from these experiments is that treatment of the cells with IFN-β before virus infection (IFN-β priming) would increase the number of expressing cells and the number of expressing alleles. Indeed, Figure 5D shows that IFN-β priming doubles the number of expressing cells and increases the number of alleles expressing the *IFN-β* gene, without affecting the frequency of interchromosomal interactions (data not shown). Thus, the IFN-β signaling-dependent effect is mediated by the IRF-7 transcription factor.

4C Isolated Loci Increase the Probability for IFN-β Expression

If the early monoallelic expression of the *IFN-β* gene in a small cell population depends on the stochastic nature of the interchromosomal interactions between the *IFN-β* gene and the 4C isolated loci, then increasing the copy number of any of the 4C clones might increase the number of the cells expressing IFN-β predominantly from a single allele. To test this idea we transfected HeLa cells with a bluescript vector harboring the #21, #9, and #14 clones, followed by virus infection. Figure 6A shows that transfection of any of the 4C plasmids increased the levels of *IFN-β* and *IκBα* gene expression after virus infection from 3- to 5-fold. As a control, we showed that the levels of *IL-8* expression were not affected, a result consistent with the fact that the *IL-8* gene does not interact with the 4C clones. Importantly, 3C experiments confirmed that the transfected 4C plasmids interact specifically with the endogenous *IFN-β* locus in a virus-infection-dependent manner (data not shown). Figure 6B shows that at least part of the *IFN-β* RNA increase is due to an increase in the number of cells expressing *IFN-β* RNA. Transfection of a construct derived from #21 harboring just the AluSX repeat also led to an increase in the number of cells expressing IFN-β but to a lesser extent than the full-length #21. Remarkably, transfection of a #21 construct harboring a precise deletion of the nonconsensus NF-κB site marginally only affected *IFN-β* RNA levels or the number of cells expressing the gene (Figures 6A and 6B). Thus, the NF-κB site of the 4C clones plays a critical role in determining the probability of IFN-β expression in each cell. One possibility could be that NF-κB associates first with the 4C clones and then is transferred to the *IFN-β* locus via interchromosomal interactions. Indeed, chromatin immunoprecipitation experiments revealed that NF-κB binds to the 4C clones earlier after virus infection than it binds to the *IFN-β* promoter (Figure 6C). More specifically, at 1 hr after virus infection NF-κB associates with the 4C clones, whereas at the same time binding at the *IFN-β* promoter is not detected (Figure 6C, lane 2). Maximal NF-κB binding to DNA corresponding to the 4C clones (lane 5) correlates with the maximal frequency of interchromosomal associations with the *IFN-β* locus (4 hr), and this correlates also with maximal recruitment of NF-κB to the *IFN-β* promoter.

To determine the ratio of mono- to multiallelic *IFN-β* gene expression after transfection of the 4C clones we carried out DNA-RNA FISH experiments on virus-infected HeLa cells. Figure 6D shows that transfection of the 4C clone #21 increased the probability of expression without affecting significantly the ratio of mono to multiallelic expression at 6 hr post-infection. The specificity of this phenomenon was underscored by the inability of the mutant 4C #21 (ΔNF-κB) to increase the number of expressing cells. A qualitatively similar result was obtained when we transfected NF-κB or IRF-7 expressing vectors (Figure 6D), an observation consistent with the fact that these factors are limiting in the cells. However, when both factors were expressed at high levels within the cells, *IFN-β* transcription began simultaneously at many more cells and at more than one allele per cell and only in virus-infected cells, further underscoring the requirement for assembly of a complete enhanceosome.

DISCUSSION

In this study we present evidence for a model to explain how virus infection induces the stochastic expression of the *IFN-β* gene (Figure 7). According to this model, the choice of the allele to be expressed depends on stochastic interchromosomal associations between the *IFN-β* gene and at least one of the three identified distinct genomic loci that could mediate binding of the transcription factor NF-κB to the *IFN-β* enhancer. Then, NF-κB nucleates enhanceosome assembly, a prerequisite for chromatin remodeling, and activation of transcription from this allele. The secreted IFN-β protein acts in a paracrine and autocrine manner to signal the presence of virus infection by inducing the expression of hundreds of genes that together establish the "antiviral state" (Stetson and Medzhitov, 2006). One of the genes activated by IFN-β is *IRF-7*, a transcription factor that associates with the IFN-β enhanceosome late in infection. The increased intracellular levels of IRF-7 trigger enhanceosome assembly in additional cells and on multiple *IFN-β* alleles in each cell, thus amplifying the production of IFN-β. This second phase of *IFN-β* transcription occurs independently of interchromosomal associations (Figure 7).

The precise organization of the *IFN-β* enhanceosome is required for optimal cooperative occupancy in response to viral

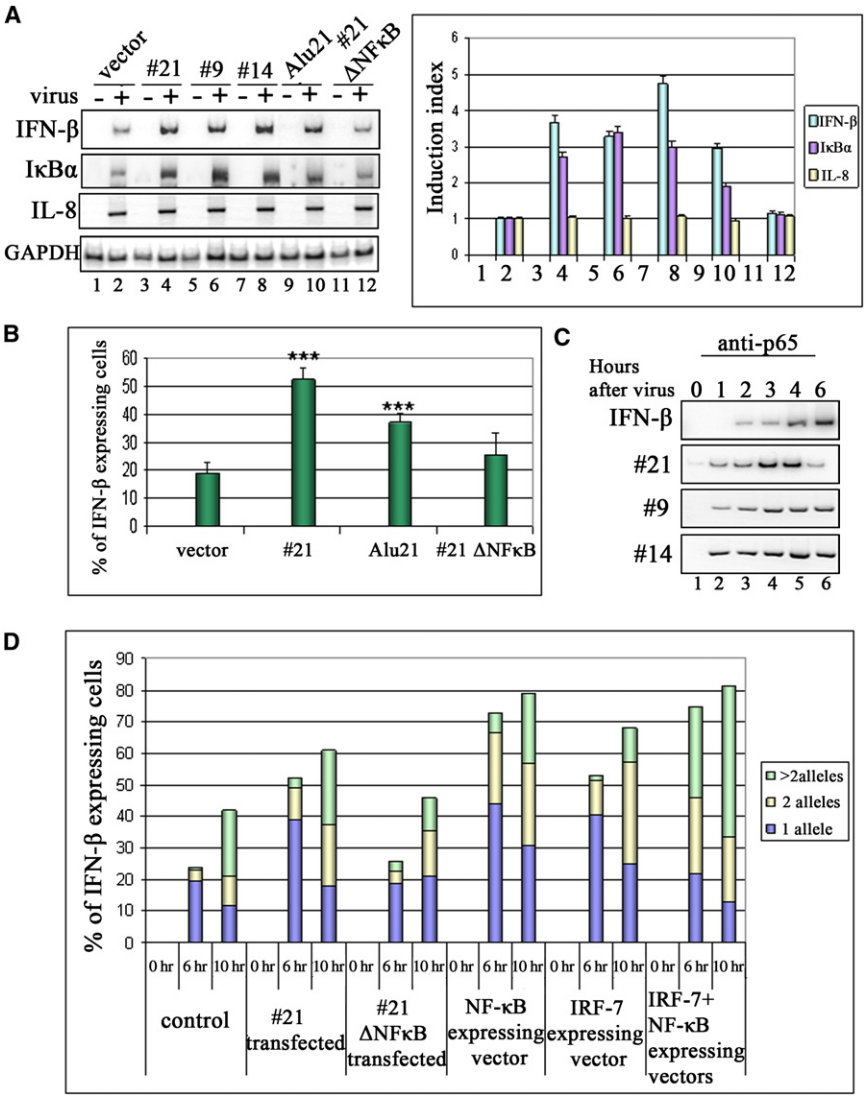

Figure 6. 4C-ChIP Clones Increase the Probability of Stochastic *IFN-β* Gene Expression

(A) HeLa cells were transfected with bluescript–based constructs bearing the 4C-ChIP clones #21, #9, and #14, a derivative of #21 containing only the Alu SX (Alu21) repeat or, a mutant of #21 lacking the NF-κB site (#21ΔNF-κB). The cells were infected with virus for 6 hr and the isolated RNA was used as a template for RT-PCR analysis using primers specific for *IFN-β*, *IκBα*, and *IL-8* genes. The radioactive bands were quantitated using phosphorImager and the data from four independent experiments were plotted and are shown at the right panel of the figure (shown are mean values ± SD).

(B) Diagrammatic representation of the percentage (mean ± SD) of cells expressing IFN-β from three independent in situ hybridization experiments performed as in Figure 1 except that the cells were transfected with the indicated bluescript-based constructs. All cells for each category were scored blindly and at least 300 cells were counted in each case. *** denotes $p < 0.001$.

(C) Crosslinked chromatin prepared from mock- or virus-infected HeLa cells for the indicated amount of time was immunoprecipitated with the p65-specific antibody. The precipitated *IFN-β* promoter and #21, #14, and #9 loci were detected by PCR using ^{32}P-dCTP in the reaction.

(D) Diagrammatic representation of the percentage of cells and the number of *IFN-β*-expressing alleles per cell from two independent RNA/DNA FISH experiments performed as in Figure 4 except that the cells were transfected with the indicated plasmids. All cells for each category were scored blindly and at least 180 cells were counted in each case. In each column the relative percentage of cells expressing 1, 2, or more *IFN-β* alleles is indicated with different colors.

infection in vivo, and it has been suggested that such an organization may reflect regulation by limiting concentrations of one or more critical activators (Papatsenko and Levine, 2007). The low concentration of NF-κB and IRF-7 explains the ordinary requirement for cooperativity in enhanceosome assembly and sets the stage for combinatorial control of transcription. On the other hand this poses a problem, that is, how to target a low abundance factor like NF-κB to the correct gene for nucleating enhanceosome assembly in a nucleus containing millions of putative NF-κB binding sites.

We have identified three genomic loci that interact separately or in combinations with a single allele of *IFN-β* (Figures 7A and 7B) in response to virus infection. Two of these loci map in different chromosomes than the *IFN-β* gene, whereas the third is on the same chromosome but on the other arm. We have been unable to clone additional loci interacting with *IFN-β* with the 4C-ChIP approach, presumably due to the high false negative rate of the approach. However, this does not exclude the possibility that the *IFN-β* locus can interact with additional loci with lower frequencies and affinities. The physical association of these distant DNA sequences with the IFN-β gene occurs during the time of enhanceosome assembly and before initiation of transcription. Thus, it is possible that these interchromosomal associations play a role in enhanceosome assembly by facilitating (delivering) NF-κB binding to the *IFN-β* promoter. The following observations are consistent with this model. First, chromatin immunoprecipitation experiments revealed that NF-κB binds to the 4C clones before binding to the *IFN-β* promoter. Second, the interchromosomal interactions are NF-κB dependent as revealed by transfecting the cells with a dominant-negative form of IκBα (ΔN-IκBα), leading to a dramatic decrease of both virus-inducible interchromosomal interactions and IFN-β expression (Figure S4). The third observation supporting a role of the 4C clones in delivering NF-κB is the experiment shown in Figure S5. We transfected p65 followed by virus infection and found a significant decrease in the frequency of interchromosomal interactions, thus suggesting that these associations take place only when the concentration of NF-κB within the cells is at

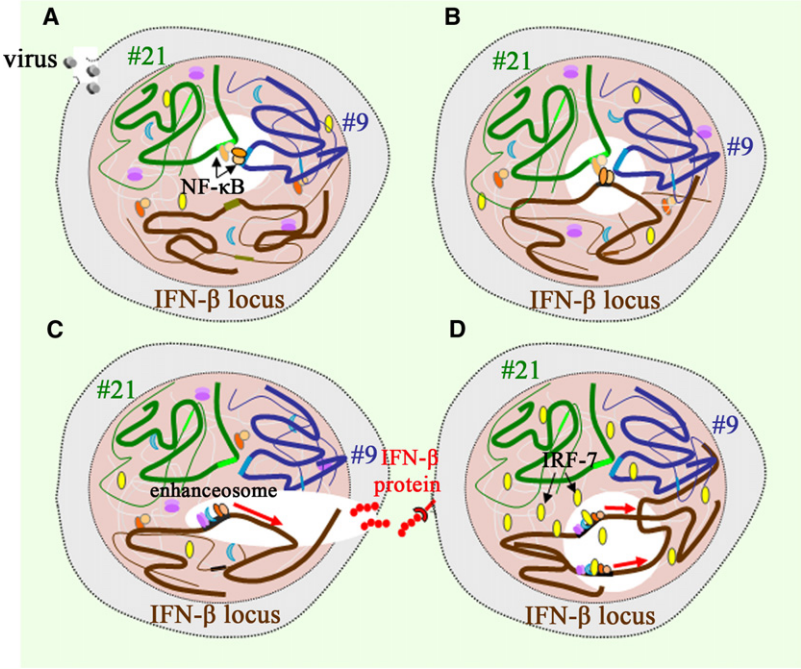

Figure 7. A Model Depicting Stochastic Activation of *IFN-β* Gene Transcription

(A) Virus infection induces the nuclear localization of NF-κB, which binds first to a site in the nucleus where single alleles of the 4C-ChIP loci are in physical proximity.

(B) Next, one allele of *IFN-β* interacts with the 4C-ChIP loci and NF-κB is transferred to the *IFN-β* enhancer. This stochastic reactions takes place in ~20% of the cells and involves a single *IFN-β* allele.

(C) NF-κB nucleates enhanceosome assembly on this allele leading to monoallelic activation of transcription.

(D) The secreted IFN-β protein acts on the same and on other not initially expressing cells to induce high-level transcription of IRF-7. The IRF-7 protein accumulates at high levels and binds to the *IFN-β* enhancer stimulating enhanceosome assembly on more than one allele. This leads to multiallelic expression and amplification of the virus infection-induced signal.

physiological low levels. Furthermore, the observation that these loci are in physical proximity before the entrance of NF-κB into the nucleus suggests that it is the *IFN-β* gene that is recruited to this site to "receive" NF-κB. When the levels of NF-κB are increased by transfection, the factor can bind to the *IFN-β* promoter independently of interchromosomal associations. We propose the existence of an NF-κB "receptor" center consisting of the 4C loci that can immediately receive NF-κB and distribute the factor to the promoters of selected genes via interchromosomal associations. We can imagine that the NF-κB receptor center is localized in specialized nuclear regions to which the incoming NF-κB can have instant access. Support for such a model comes from the fact that the affinity of NF-κB for these sites is 2–3 times lower than that for the *IFN-β* gene (our unpublished data), thus implying that its preference for the receptor center could be due to a combination of factors such as the local nuclear architecture, DNA-induced allostery, and/or other proteins localized in this microenvironment. We do not know the mechanisms assuring the specificity of these interchromosomal associations since not all NF-κB-regulated genes (e.g., *IL-8*) are recruited to the NF-κB center. It is possible that additional factors bound to the 4C clones and/or to the promoters of the recruited genes determine the specificity of the interactions by exposing complementary surfaces. A prediction derived from our model is that conversion of the low-affinity specialized NF-κB site present in the 4C clones to a consensus high-affinity site would preclude the delivery of NF-κB to the *IFN-β* enhancer, resulting in a decrease in transcription. Figure S6 shows that the 4C clones bearing a consensus high-affinity NF-κB site taken from the MHC class I are not only incapable of facilitating *IFN-β* expression but also decrease *IFN-β* transcription, presumably by serving as competitors. Additional support for our model is provided by the observation that all 4C clones contain specialized Alu repeats, and that the Alu NF-κB site is an integral functional component of the repeats required for the stochastic IFN-β expression. Previous studies have shown that Alu repeats are euchromatic and contain several functional transcription factor-binding sites and may play a role in regulation of biological processes (Polak and Domany, 2006). We can imagine that Alu repeats interspersed in the genome may function as "marks" to properly align interacting chromosomal domains during the execution of several nuclear processes.

The model we propose stipulates that the stochastic activation of only one allele is dependent on the limited concentration of NF-κB, and it could explain the monoallelic and stochastic expression of many other cytokines regulated by NF-κB. Furthermore, the stochastic oscillation of NF-κB in individual cells further underscores the requirement for a promoter-targeting mechanism to ensure the proper activation of immune genes (Nelson et al., 2004). The formation of a complex between *IFN-β* and the 4C clones is a rapid signal-dependent process that occurs within 2 hr of virus infection, thus differing from other types of interchromosomal interactions described in olfactory receptor expression (Lomvardas et al., 2006), T cell differentiation (Spilianakis et al., 2005), HoxB1-dependent ES differentiation (Wurtele and Chartrand, 2006), imprinting (Ling et al., 2006; Zhao et al., 2006), erythroid gene expression (Osborne et al., 2004), X chromosome inactivation (Bacher et al., 2006; Xu et al., 2006), etc., which are established during long-lasting cell differentiation pathways. Furthermore, the interchromosomal interactions described here occur between a known gene and intergenic loci with previously unknown function.

The monoallelically produced and secreted IFN-β protein activates among others the *IFN-β* gene activator IRF-7. Before virus infection, IRF-7 is expressed at very low amounts and has a very short half-life, and, like IRF-3, virus infection induces serine phosphorylation allowing IRF-7's dimerization and nuclear translocation (Honda et al., 2006). This observation is consistent with our siRNA experiments, which revealed a small contribution of IRF-7 in the initial monoallelic expression of *IFN-β* but

underscored its role in late multiallelic *IFN-β* transcription. We believe that the high levels of IRF-7 production in response to IFN-β signaling drive enhanceosome assembly in more cells and in more than one allele per cell (Figure 7D). As predicted, IRF-7 overexpression experiments and IFN priming increased the number of expressing cells and alleles. In other words, the "pioneer" factor that nucleates enhaceosome assembly in the second phase appears to be IRF-7 as opposed to NF-κB in the first phase.

In summary, we present evidence that the limiting factor NF-κB is delivered to a single *IFN-β* allele via stochastic interchromosomal associations, and this nucleates enhanceosome assembly by "recruiting" the remaining factors via DNA-induced conformational changes and protein-protein interactions leading to transcriptional activation. Next, the remaining *IFN-β* alleles are activated through the IRF-7-driven assembly of enhanceosomes and independently of interchromosomal associations (Figure 7). Consistent with this idea is our observation that overexpression of both p65 and IRF-7 leads to the simultaneous expression of *IFN-β* from multiple alleles even at the early phase of expression. Thus, our experiments provided a mechanistic model of how the *IFN-β* enhancer integrates inputs received from virus infection and signal amplification derived from the positive IFN feedback loop.

EXPERIMENTAL PROCEDURES

Tissue Culture and Cell Transfection and In Situ Hybridization

HeLa CCL-2 (ATCC) and HCT-116 cells were cultured in DMEM supplemented with 10% FBS and 1% PENSTREP at 37°C. All transfections were performed with lipofectamine 2000 (Invitrogen) according to the manufacturer's instructions. Cells transfected with siRNA for IRF-7 (sc-38011, SantaCruz Biotechnology) were grown for 62 hr before virus infection. In situ hybridizations were performed as described previously (Senger et al., 2000).

3C and 4C-ChIP

The 3C analysis was performed as described previously (Dekker et al., 2002). The detailed procedure is described in the Supplemental Data. For the 4C-ChIP, the cells were treated as in the 3C. After EcoRI restriction, the cleaved chromatin was dialyzed in a buffer containing 5% glycerol, 10 mM Tris-HCl (pH 8), 1 mM EDTA, and 0.5 mM EGTA overnight (O/N) at 4°C. Fifty micrograms of the chromatin was used for immunoprecipitation with the anti-p65 antibody as previously described (Agelopoulos and Thanos, 2006). After the final wash with TE, a small sample of the beads was removed in order to check the ChIP efficiency. The bead-bound fragments were ligated O/N, at 16°C with 100 U of ligase in 1 ml final volume, followed by addition of ligase and ATP and incubation at room temperature (RT) for 3 hr. The immunoprecipitated and ligated DNA was isolated and used as template for inverse-nested PCR (Figure S5). The products were analyzed and isolated from a 1.5% agarose gel and cloned in pGEM Teasy vector (Promega), and the positive clones were analyzed by DNA sequencing.

DNA and DNA/RNA FISH

The DNA FISH analysis was performed as described in the Supplemental Data. The BAC probes used were obtained from CHORI BACPAC libraries. Specifically we used the following: RPCI-11.113D19 for the *IFN-β* locus, RPCI-11.447E20 for the *IL-8* locus, RPCI-11.395I6 for #21, RPCI-11.81F13 for *IκBα*, RPCI-11.418K9 for #9, RPCI-11.430N14 for #14, and CTB-BRI 64I22 for the AluSx control clone. For the DNA/RNA FISH, the cells were attached on glass slides, were washed with ice-cold PBS, and incubated for 10 min in cytoskeleton buffer containing 100 mM NaCl, 300 mM sucrose, 3 mM $MgCl_2$, 10 mM Pipes, 0.1% Triton X-100, and 20 mM vanadyl-ribonucleoside, and were then fixed for 15 min at RT in a solution containing 4% PFA in PBS with 5% acetic acid. The slides were then incubated overnight in 70% ethanol at 4°C. The next day the permeabilized cells were incubated in 50% formamide-2× SSC at 70°C for 3 min and dried in ethanol series. The probes after heat denaturation were applied directly on the dried cells and incubated O/N at 37°C. The slides were washed two times for 10 min in a solution of 50% formamide in 2× SSC at 37°C. After 30 min of blocking at RT the signal was detected with incubation of anti-DIG/ Fluorescein antibody or streptavidin/ Alexa 568 in a solution containing 0.1 M Tris-HCl (pH 8), 0.15 M NaCl, 1× blocking reagent (Roche), and 20 mM vanadyl-ribonucleoside complex. The antibody was crosslinked in 4% PFA in PBS for 10 min at RT. Then DNA FISH was performed using the NaOH denaturation protocol described above.

SUPPLEMENTAL DATA

Supplemental Data include Supplemental Experimental Procedures and seven figures and can be found with this article online at http://www.cell.com/cgi/content/full/134/1/85/DC1/.

ACKNOWLEDGMENTS

We thank Sarantis Gagos for help with the DNA FISH and Marios Agelopoulos for advice with the ChIP experiments. We also thank Tom Maniatis, Richard Mann, Stavros Lomvardas, Ethan Ford, Mat Lavigne, George Panayotou, and George Mosialos for critical reading of the manuscript. This work was supported from grants to D.T. from the Greek Secreteriat for Research and Technology (03PENED-422), March of Dimes, Association for International Cancer Research, and EU (FP6 Transfog). E.A. was partially supported from the Greek National Foundation of Scholarships.

Received: December 21, 2007
Revised: March 18, 2008
Accepted: May 3, 2008
Published: July 10, 2008

REFERENCES

Agalioti, T., Lomvardas, S., Parekh, B., Yie, J., Maniatis, T., and Thanos, D. (2000). Ordered recruitment of chromatin modifying and general transcription factors to the IFN-beta promoter. Cell *103*, 667–678.

Agelopoulos, M., and Thanos, D. (2006). Epigenetic determination of a cell-specific gene expression program by ATF-2 and the histone variant macroH2A. EMBO J. *25*, 4843–4853.

Bacher, C.P., Guggiari, M., Brors, B., Augui, S., Clerc, P., Avner, P., Eils, R., and Heard, E. (2006). Transient colocalization of X-inactivation centres accompanies the initiation of X inactivation. Nat. Cell Biol. *8*, 293–299.

Calado, D.P., Paixao, T., Holmberg, D., and Haury, M. (2006). Stochastic monoallelic expression of IL-10 in T cells. J. Immunol. *177*, 5358–5364.

Dekker, J., Rippe, K., Dekker, M., and Kleckner, N. (2002). Capturing chromosome conformation. Science *295*, 1306–1311.

de Laat, W., and Grosveld, F. (2007). Inter-chromosomal gene regulation in the mammalian cell nucleus. Curr. Opin. Genet. Dev. *17*, 456–464.

Enoch, T., Zinn, K., and Maniatis, T. (1986). Activation of the human β-interferon gene requires an interferon-inducible factor. Mol. Cell. Biol. *6*, 801–810.

Escalante, C.R., Nistal-Villan, E., Shen, L., Garcia-Sastre, A., and Aggarwal, A.K. (2007). Structure of IRF-3 bound to the PRDIII-I element of the human interferon−βeta enhancer. Mol. Cell *26*, 703–716.

Guo, L., Hu-Li, J., and Paul, W.E. (2005). Probabilistic regulation in TH2 cells accounts for monoallelic expression of IL-4 and IL-13. Immunity *23*, 89–99.

Holländer, G.A., Zuklys, S., Morel, C., Mizoguchi, E., Mobisson, K., Simpson, S., Terhorst, C., Wishart, W., Golan, D.E., Bhan, A.K., and Burakoff, S.J. (1998). Monoallelic expression of the interleukin-2 locus. Science *279*, 2118–2121.

Honda, K., Takaoka, A., and Taniguchi, T. (2006). Type I interferon gene induction by the interferon regulatory factor family of transcription factors. Immunity *25*, 349–360.

Hottiger, M.O., Felzien, L.K., and Nabel, G.J. (1998). Modulation of cytokine-induced HIV gene expression by competitive binding of transcription factors to the coactivator p300. EMBO J. *17*, 3124–3134.

Hu, J., Sealfon, S.C., Hayot, F., Jayaprakash, C., Kumar, M., Pendleton, A.C., Ganee, A., Fernandez-Sesma, A., Moran, T.M., and Wetmur, J.G. (2007). Chromosome-specific and noisy IFNB1 transcription in individual virus-infected human primary dendritic cells. Nucleic Acids Res. *35*, 5232–5241.

Kelly, B.L., and Locksley, R.M. (2000). Coordinate regulation of the IL-4, IL-13, and IL-5 cytokine cluster in Th2 clones revealed by allelic expression patterns. J. Immunol. *165*, 2982–2986.

Ling, J.Q., Li, T., Hu, J.F., Vu, T.H., Chen, H.L., Qiu, X.W., Cherry, A.M., and Hoffman, A.R. (2006). CTCF mediates interchromosomal colocalization between Igf2/H19 and Wsb1/Nf1. Science *312*, 269–272.

Lipniacki, T., Paszek, P., Brasier, A.R., Luxon, B.A., and Kimmel, M. (2006). Stochastic regulation in early immune response. Biophys. J. *90*, 725–742.

Lomvardas, S., and Thanos, D. (2001). Nucleosome sliding via TBP DNA binding in vivo. Cell *106*, 685–696.

Lomvardas, S., and Thanos, D. (2002). Modifying gene expression programs by altering core promoter chromatin architecture. Cell *110*, 261–271.

Lomvardas, S., Barnea, G., Pisapia, D.J., Mendelsohn, M., Kirkland, J., and Axel, R. (2006). Interchromosomal interactions and olfactory receptor choice. Cell *126*, 403–413.

Maniatis, T., Falvo, J.V., Kim, T.H., Kim, T.K., Lin, C.H., Parekh, B.S., and Wathelet, M.G. (1998). Structure and function of the interferon–beta enhanceosome. Cold Spring Harb. Symp. Quant. Biol. *63*, 609–620.

Misteli, T. (2007). Beyond the sequence: cellular organization of genome function. Cell *128*, 787–800.

Munshi, N., Yie, Y., Merika, M., Senger, K., Lomvardas, S., Agalioti, T., and Thanos, D. (1999). The IFN–beta enhancer: a paradigm for understanding activation and repression of inducible gene expression. Cold Spring Harb. Symp. Quant. Biol. *64*, 149–159.

Munshi, N., Agalioti, T., Lomvardas, S., Merika, M., Chen, G., and Thanos, D. (2001). Coordination of a transcriptional switch by HMGI(Y) acetylation. Science *293*, 1133–1136.

Nelson, D.E., Ihekwaba, A.E., Elliott, M., Johnson, J.R., Gibney, C.A., Foreman, B.E., Nelson, G., See, V., Horton, C.A., Spiller, D.G., et al. (2004). Oscillations in NF–κappaB signaling control the dynamics of gene expression. Science *306*, 704–708.

Osborne, C., Chakalova, L., Brown, K.E., Carter, D., Horton, A., Debrand, E., Goyenechea, B., Mitchell, J.A., Lopes, S., Reik, W., and Fraser, P. (2004). Active genes dynamically colocalize to shared sites of ongoing transcription. Nat. Genet. *36*, 1065–1069.

Panne, D., Maniatis, T., and Harrison, S.C. (2007). An atomic model of the interferon–βeta enhanceosome. Cell *129*, 1111–1123.

Papatsenko, D., and Levine, M. (2007). A rationale for the enhanceosome and other evolutionarily constrained enhancers. Curr. Biol. *17*, R955–R957.

Paun, A., and Pitha, P.M. (2007). The innate antiviral response: new insights into a continuing story. Adv. Virus Res. *69*, 1–66.

Polak, P., and Domany, E. (2006). Alu elements contain many binding sites for transcription factors and may play a role in regulation of developmental processes. BMC Genomics *7*, 133.

Riviere, I., Sunshine, M.J., and Littman, D.R. (1998). Regulation of IL-4 expression by activation of individual alleles. Immunity *9*, 217–228.

Sato, M., Suemori, H., Hata, N., Asagiri, M., Ogasawara, K., Nakao, K., Nakaya, T., Katsuki, M., Noguchi, S., Tanaka, N., et al. (2000). Distinct and essential roles of transcription factors IRF-3 and IRF-7 in response to viruses for IFN-alpha/beta gene induction. Immunity *13*, 539–548.

Senger, K., Merika, M., Agalioti, T., Yie, J., Escalante, C.R., Chen, G., Aggarwal, A.K., and Thanos, D. (2000). Gene repression by coactivator repulsion. Mol. Cell *6*, 931–937.

Spilianakis, C.G., Lalioti, M.D., Town, T., Lee, G.R., and Flavell, R.A. (2005). Interchromosomal associations between alternatively expressed loci. Nature *435*, 637–645.

Stetson, D.B., and Medzhitov, R. (2006). Types I interferons in host defense. Immunity *25*, 373–381.

Taniguchi, T., and Takaoka, A. (2002). The interferon-alpha/beta system in antiviral responses: a multimodal machinery of gene regulation by the IRF family of transcription factors. Curr. Opin. Immunol. *14*, 111–116.

Thanos, D., and Maniatis, T. (1995). Virus induction of human IFN beta gene expression requires the assembly of an enhanceosome. Cell *83*, 1091–1100.

Wurtele, H., and Chartrand, P. (2006). Genome-wide scanning of HoxB1-associated loci in mouse ES cells using an open-ended Chromosome Conformation Capture methodology. Chromosome Res. *14*, 477–495.

Xu, N., Tsai, C.L., and Lee, J.T. (2006). Transient homologous chromosome pairing marks the onset of X inactivation. Science *311*, 1149–1152.

Zawatzky, R., De Maeyer, E., and De Maeyer-Guignard, J. (1985). Identification of individual interferon-producing cells by in situ hybridiazation. Proc. Natl. Acad. Sci. USA *82*, 1136–1140.

Zhao, Z., Tavoosidana, G., Sjolinder, M., Gondor, A., Mariano, P., Wang, S., Kanduri, C., Lezcano, M., Sandhu, K.S., Singh, U., et al. (2006). Circular chromosome conformation capture (4C) uncovers extensive networks of epigenetically regulated intra- and interchromosomal interactions. Nat. Genet. *38*, 1341–1347.

OPEN ACCESS Freely available online

PLoS PATHOGENS

IPS-1 Is Essential for the Control of West Nile Virus Infection and Immunity

Mehul S. Suthar[1], Daphne Y. Ma[1☯], Sunil Thomas[1☯], Jennifer M. Lund[1¤a], Nu Zhang[1], Stephane Daffis[2], Alexander Y. Rudensky[1¤b], Michael J. Bevan[1], Edward A. Clark[1,3], Murali-Krishna Kaja[1], Michael S. Diamond[2], Michael Gale Jr.[1,3]*

1 Department of Immunology, University of Washington School of Medicine, Seattle, Washington, United States of America, **2** Departments of Medicine, Molecular Microbiology, and Pathology and Immunology, Washington University School of Medicine, St. Louis, Missouri, United States of America, **3** Department of Microbiology, University of Washington School of Medicine, Seattle, Washington, United States of America

Abstract

The innate immune response is essential for controlling West Nile virus (WNV) infection but how this response is propagated and regulates adaptive immunity *in vivo* are not defined. Herein, we show that IPS-1, the central adaptor protein to RIG-I-like receptor (RLR) signaling, is essential for triggering of innate immunity and for effective development and regulation of adaptive immunity against pathogenic WNV. IPS-$1^{-/-}$ mice exhibited increased susceptibility to WNV infection marked by enhanced viral replication and dissemination with early viral entry into the CNS. Infection of cultured bone-marrow (BM) derived dendritic cells (DCs), macrophages (Macs), and primary cortical neurons showed that the IPS-1-dependent RLR signaling was essential for triggering IFN defenses and controlling virus replication in these key target cells of infection. Intriguingly, infected IPS-$1^{-/-}$ mice displayed uncontrolled inflammation that included elevated systemic type I IFN, proinflammatory cytokine and chemokine responses, increased numbers of inflammatory DCs, enhanced humoral responses marked by complete loss of virus neutralization activity, and increased numbers of virus-specific CD8+ T cells and non-specific immune cell proliferation in the periphery and in the CNS. This uncontrolled inflammatory response was associated with a lack of regulatory T cell expansion that normally occurs during acute WNV infection. Thus, the enhanced inflammatory response in the absence of IPS-1 was coupled with a failure to protect against WNV infection. Our data define an innate/adaptive immune interface mediated through IPS-1-dependent RLR signaling that regulates the quantity, quality, and balance of the immune response to WNV infection.

Citation: Suthar MS, Ma DY, Thomas S, Lund JM, Zhang N, et al. (2010) IPS-1 Is Essential for the Control of West Nile Virus Infection and Immunity. PLoS Pathog 6(2): e1000757. doi:10.1371/journal.ppat.1000757

Editor: Ralph S. Baric, University of North Carolina, United States of America

Received July 29, 2009; **Accepted** January 7, 2010; **Published** February 5, 2010

Funding: This work was supported by NIH grants T32AI007411 (M.S.S.), AI057568, and AI083019, funds from the State of Washington (M.G.), and Washington University School of Medicine Departmental Funds (M.S.D.). The funders had no role in study design, data collection and analysis, decision to publish, or preparation of the manuscript.

Competing Interests: The authors have declared that no competing interests exist.

* E-mail: mgale@u.washington.edu

☯ These authors contributed equally to this work.

¤a Current address: Vaccine and Infectious Disease Institute, Fred Hutchinson Cancer Research Center, Seattle, Washington, United States of America
¤b Current address: Department of Immunology, Sloan-Kettering Institute, Memorial Sloan-Kettering Cancer Center, New York, New York, United States of America

Introduction

West Nile virus (WNV) is a neurotropic flavivirus and is an emerging public health threat. Infection with WNV now constitutes the leading cause of mosquito-borne and epidemic encephalitis in humans in the United States [1]. WNV is enveloped and contains a single strand positive sense RNA genome of approximately 11 kb in length that encodes three structural (C, prM/M, and E) and seven non-structural proteins (NS1, NS2A, NS2B, NS3, NS4A, NS4B, and NS5). It cycles enzootically between birds and *Culex* mosquitoes, with humans infected as dead-end hosts. WNV infection has been modeled in inbred mice wherein infection and pathogenesis recapitulate many of the features of human infection (reviewed in [2]). Following subcutaneous inoculation, WNV replicates in dendritic cells (DCs) at the portal of entry and in the draining lymph node. A primary viremia develops and virus spreads to visceral organs including the spleen, where further amplification occurs, leading to central nervous system (CNS) dissemination and encephalitis. In humans, WNV causes an acute febrile illness that can progress to severe and sometimes lethal neuroinvasive disease, especially in the elderly and immunocompromised [3]. However, healthy young adults are also afflicted with severe neurological disease [4,5,6], indicating that virulence can occur independently of immune deficiencies or aging.

Intracellular innate immune defenses and the actions of type I interferon (IFN) provide a first-line of defense against virus infection and are essential for the control of WNV replication, dissemination, and neurovirulence [7]. Innate antiviral immune defenses are triggered through the recognition of conserved pathogen associated molecular pattern (PAMP) motifs within viral products by intracellular pathogen recognition receptor (PRR) proteins in infected cells. PRR signaling directs downstream activation of latent

Author Summary

West Nile virus (WNV) is a mosquito-transmitted RNA virus that has emerged in the Western hemisphere and is now the leading cause of arboviral encephalitis in the United States. However, the virus/host interface that controls WNV pathogenesis is not well understood. Previous studies have established that the innate immune response and interferon (IFN) defenses are essential for controlling virus replication and dissemination. In this study, we assessed the importance of the RIG-I like receptor (RLR) signaling pathway in WNV pathogenesis through analysis of mice lacking IPS-1, the central adaptor molecule of RLR signaling. Our studies revealed that IPS-1 is essential for protection against WNV infection and that it regulates processes that control virus replication and triggering of innate immune defenses. We found that IPS-1 plays an important role in establishing adaptive immunity through an innate/adaptive interface that elicits effective antibody responses and controls the expansion of regulatory T cells. Thus, RLRs are essential for pathogen recognition of WNV infection and their signaling programs help orchestrate immune response maturation, regulation of inflammation, and immune homeostasis that define the outcome of WNV infection.

transcription factors, including NF-κB, interferon regulatory factor (IRF)-3 and IRF-7, in a cell type-specific manner to induce antiviral response programs that include expression of proinflammatory cytokines, chemokines, type I IFN, and interferon stimulated genes (ISGs) [7,8,9,10]. The ISG products induced through autocrine and paracrine actions of IFN confer antiviral activity by limiting virus replication and cell-to-cell virus spread. Modulation of IFN signaling has been identified as a virulence feature of pathogenic strains of WNV [11,12].

The RLRs, retinoic acid inducible gene-I (RIG-I) and melanoma differentiation antigen 5 (MDA5) [13,14,15,16], are PRRs that play critical roles in triggering immune defenses against RNA virus infection, including WNV. RIG-I and MDA5 are cytosolic RNA helicases that contain an amino terminal tandem caspase activation and recruitment domain (CARD). Upon engaging RNA substrates, the RLRs undergo a conformational change and bind to the mitochondrial associated protein, interferon promoter stimulator-1 (IPS-1) through a CARD-CARD interaction, leading to IPS-1-dependent signaling of IFN production and expression of immune response genes [17,18]. RLR signaling and IPS-1 function have an essential role in triggering IFN defenses during WNV infection of mouse embryo fibroblasts (MEFs) and human cell lines *in vitro*. Cells lacking either RIG-I or MDA5 were attenuated in their ability to generate an effective innate immune response to infection, whereas cells lacking both RIG-I and MDA5 or those deficient in IPS-1 alone were unable to respond to infection with WNV and related flaviviruses [19,20,21,22]. Recent studies examined the role of another class of pattern recognition receptors, Toll like receptor (TLR)3 and TLR7, and show that these receptors are also important PRRs of WNV infection, as they play a role in signaling IFN production and an inflammatory response upon viral ligand recognition [23,24,25]. TLR3 has been shown to contribute to both enhancement and protection of CNS inflammation and neurovirulence of WNV *in vivo* [23,24], while TLR7-dependent signaling was shown to be essential for directing proper immune cell homing to sites of WNV infection during the adaptive immune response *in vivo* [25].

Type I IFN, a major product of PRR signaling, has been shown to link innate and adaptive immune responses. However, the specific PRR pathways that mediate this during acute WNV infection have not been delineated nor has the RLR pathway been evaluated in this context. The quantity and quality of the innate and adaptive immune responses after infection must be carefully regulated to avoid aberrant inflammation and immunopathogenesis. Regulatory T (T_{reg}) cells and inflammatory dendritic cell (DC) subsets regulate inflammation during acute virus infection through T cell suppression and by modulating the trafficking and inflammatory cytokine production of immune cells into infected tissues [26,27,28]. Thus, the level of local and peripheral T_{reg} cells, and the composition of local DC subsets that develop during WNV infection may determine immune control and WNV disease.

Here, we assessed the role of RLR signaling and IPS-1 in WNV infection and immunity. Our studies define IPS-1 as an essential modulator of immunity *in vivo* and demonstrate that IPS-1-dependent signaling orchestrates an innate/adaptive immune interface that regulates immune responses to effectively control WNV infection.

Results

RIG-I and IPS-1 are essential for protection against WNV infection

WNV infection of primary embryonic fibroblasts recovered from RIG-I$^{-/-}$ mice revealed that RIG-I was important in eliciting innate antiviral immune defenses early during infection, whereas MDA5 was important for enhancing and sustaining this response [21]. We further evaluated WNV infection of RIG-I$^{-/-}$ or MDA5$^{-/-}$ mice and confirmed that RIG-I serves a dominant role among the RLRs for the acute induction of innate immune defenses and protection against WNV infection *in vivo* (data not shown). Since the RLRs signal innate defenses through the IPS-1 adaptor protein [29], we also examined the role of IPS-1 in protection against WNV infection upon a sub-lethal virus challenge of wild type and IPS-1$^{-/-}$ mice. IPS-1$^{-/-}$ mice were highly susceptible to WNV infection and exhibited 100% mortality with an average survival time (AST) of 7.3 days as compared to wild type mice (38.5% mortality with an AST of 13.2 days; $p<0.0001$; **Fig 1A**). Thus, RIG-I and IPS-1-dependent signaling are essential for protection against WNV infection.

IPS-1-dependent signaling controls WNV replication, tissue tropism, and CNS invasion

To define the role of IPS-1 in controlling WNV *in vivo*, wild type and IPS-1$^{-/-}$ mice were infected subcutaneously (s.c.) with 100 PFU of WN-TX and viral burden within peripheral tissues and the CNS was measured over time post-infection (pi). IPS-1$^{-/-}$ mice exhibited increased viremia compared to wild type mice (45.7 fold enhancement at day 1 pi, $P<0.05$) throughout the course of infection (**Fig 1B**). Similarly, viral loads in the spleen were elevated in the infected IPS-1$^{-/-}$ mice (**Fig 1C**). WNV infection of IPS-1$^{-/-}$ mice displayed an expanded tissue tropism as infectious virus was found in the kidneys, a tissue that is not normally permissive to infection in wild type mice (**Fig 1D**). WNV is typically detected in the CNS of wild type mice after s.c. challenge between 4 and 8 days pi [2]. Consistent with this time course, infected wild type mice exhibited detectable viral loads (average viral titer of $10^{1.8}$ pfu/gram of tissue) in the brain by day 6 p.i., although virus was not detected in the spinal cord (**Fig 1E and F**). In contrast, WNV spread to the brain (**Fig 1E**) and spinal cord of IPS-1$^{-/-}$ mice (**Fig 1F**) by day 2 pi, with viral loads rising through day 6 pi. Together these results indicate that IPS-1, likely

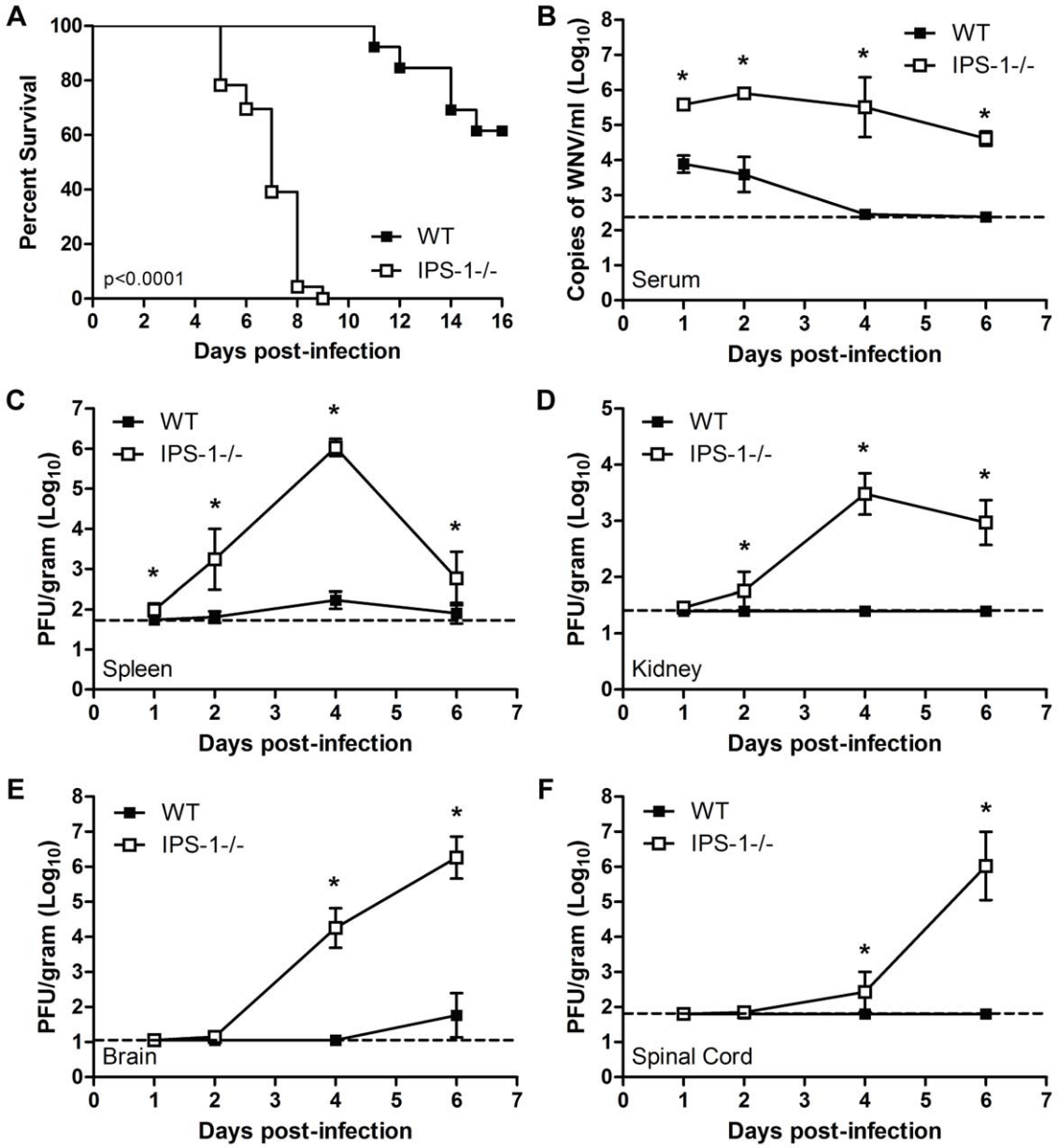

Figure 1. Virologic analysis in wild type and IPS-1$^{-/-}$ mice. Adult wild type and IPS-1$^{-/-}$ mice were infected s.c. with 100 PFU of WN-TX. (A) Differential lethality from WNV infection (WT n = 13; IPS-1$^{-/-}$ n = 23; $p<0.0001$). B–F. Viral burden analysis of peripheral and CNS tissues from wild type and IPS-1$^{-/-}$ mice infected s.c. with 100 PFU of WN-TX. (B) WNV RNA in serum and infectious virus in the (C) spleen, (D) kidney, (E) brain, and (F) spinal cord were determined by RT-qPCR assay (B) or viral plaque assay (C–F) of samples harvested on day 1, 2, 4, and 6 pi. Data are shown as copies of WNV genome RNA per ml of serum or PFU per gram of tissue for 3 to 6 mice per timepoint. Graphs show the mean +/− standard deviation for each measurement. Asterisk denotes $p<0.05$. The horizontal line indicates the lower limit of assay sensitivity.
doi:10.1371/journal.ppat.1000757.g001

through RLR signaling of innate immune defenses, limits WNV replication, viremia, and peripheral spread, and is essential for the control of viral invasion of the CNS.

IPS-1 regulates the innate immune response to WNV infection in myeloid cells

Myeloid cells, including tissue and lymphoid DC and macrophages (Mϕ), are among the first cells to encounter WNV during infection and thus function to restrict the spread of virus to distant tissues and the CNS [2]. To define the role of IPS-1 in controlling virus replication and innate immunity in myeloid cells, we analyzed WNV infection and host responses in primary bone marrow-derived DC and Mϕ recovered from wild type and IPS-1$^{-/-}$ mice. DC and Mϕ were infected at an MOI of 1.0 (relative to viral plaque assay quantification of BHK-21 cells; see Methods) and evaluated for virus replication, IFN induction, and innate immune triggering of ISG expression (**Fig 2**). IPS-1$^{-/-}$ DCs sustained significantly higher WNV replication at 36 and 48 hours pi compared to wild type infected cells (**Fig 2A**). WNV infection of wild type DCs induced IFN-β secretion but this response was completely abolished in IPS-1$^{-/-}$ DCs (**Fig 2B**). The lack of IFN-β induction in IPS-1$^{-/-}$ DCs correlated with a lack of ISG expression including RIG-I, MDA5, and STAT-1 (**Fig 2C**). In addition, expression of ISG54 and

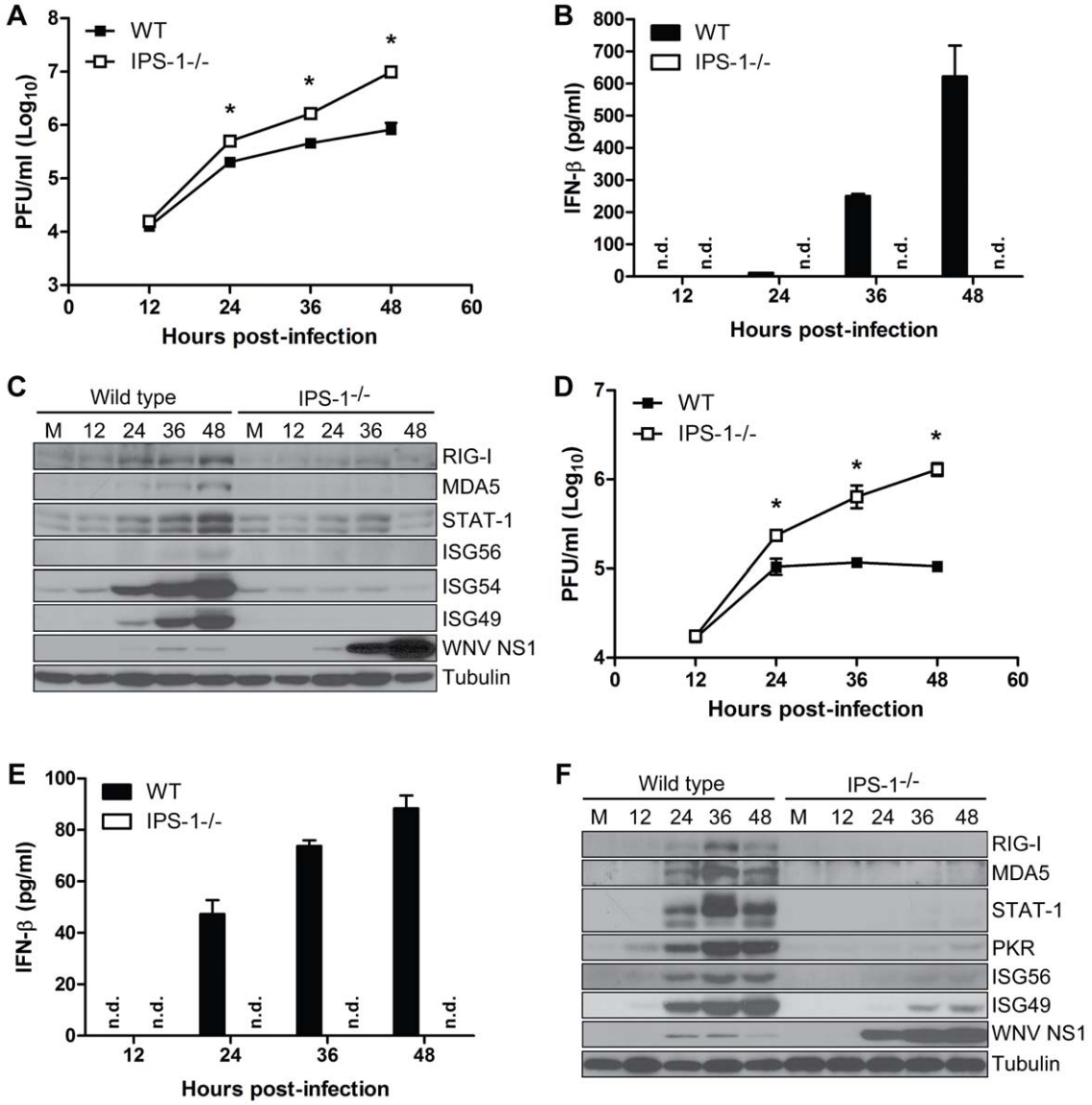

Figure 2. IPS-1 is essential for triggering the innate immune response to WNV infection and controlling virus replication in myeloid cells. Primary bone-marrow derived dendritic cells (A–C) and macrophages (D–F) recovered from wild type mice and IPS-$1^{-/-}$ mice were mock-infected (M) or infected with WN-TX at an MOI of 1.0. Cells and culture media were harvested at the times indicated pi for determination of virus load (A, D) and IFN-β production (B, E), respectively. n.d. = not detected. Graphs show the mean +/− standard deviation from three independent experiments. Asterisk denotes $p<0.05$. (C,F) Immunoblot analysis of protein abundance in lysates from mock-infected (M) and WN-TX infected cells. For panel C, STAT-1 expression in dendritic cells was normalized at each timepoint to loading control and compared to mock (relative fold induction WT, KO at 12 hours 1.72, 0.7; 24 hours 2.6, 0.8; 36 hours 4.6, 1.1; 48 hours 9.9, 0.6).
doi:10.1371/journal.ppat.1000757.g002

ISG49, which are direct IRF-3 target genes [30,31], were not induced during WNV infection of IPS-$1^{-/-}$ DCs (**Fig 2C**). Moreover, ISG56, another IRF-3 target gene [31], was induced late during infection and to lower levels as compared to ISG54 and ISG49 in wild type, infected DCs. WNV infection of IPS-$1^{-/-}$ Mϕ resulted in significantly higher virus replication between 24 and 48 hours pi as compared to infected wild type cells (**Fig 2D**). Whereas wild type infected Mϕ expressed IFN-β, this response was completely abolished in IPS-$1^{-/-}$ Mϕ (**Fig 2F**). We also observed a differential expression of ISGs and IRF-3-target genes within WNV-infected Mϕ. RIG-I, MDA5, and STAT-1 were not induced in IPS-$1^{-/-}$ Mϕ, whereas, ISG56, ISG49, and PKR were expressed at reduced levels and with delayed kinetics. These data establish that IPS-1-dependent RLR signaling is the major innate immune signaling pathway that controls virus replication in conventional DCs and Mϕ.

The RLR signaling pathway triggers the innate immune response to WNV infection in primary cortical neurons

Neurons represent the target cell of WNV infection in the CNS and their death after infection is a key factor in pathogenesis and neurological sequelae [32,33]. To define the role of RLR signaling in restricting virus replication in neurons, primary cortical neurons were generated from wild type and IPS-$1^{-/-}$ mice. Cells were infected at an MOI of 1.0 with WN-TX and virus yield, IFN-β induction, and ISG expression were evaluated. In the absence of IPS-1, WNV replicated faster and to higher levels resulting in a 2.2 and 4.2-fold ($p<0.05$) increase in viral production at 24 hrs and 48

pi, respectively as compared to infected wild type neuronal cells (**Fig 3A**). This relatively modest virologic effect in neurons compared to that observed in IPS-$1^{-/-}$ DC and Mϕ was expected, as IFN-α or -β pre-treatment only inhibits WNV infection in cortical neurons to a maximum of 5 to 8-fold [12], suggesting that the IFN response is comparably less potent in neurons. IFN-β expression was induced to lower levels in IPS-$1^{-/-}$ neurons compared to wild type infected neurons at 24 (10-fold, $p<0.05$) and 36 hours pi (5-fold, $p<0.05$) despite the higher levels of virus replication (**Fig 3A and 3B**). Expression of ISGs, (including RIG-I and MDA5) and IRF-3 target genes (including ISG56 and ISG49) followed this pattern and were dependent on IPS-1 for rapid and high level expression (**Fig 3C**). The presence of IFN-β and ISG transcripts in IPS-$1^{-/-}$ cells at 48 hrs pi is consistent with the finding that TLR3 has an independent and subordinate role in triggering innate immune responses in cortical neurons at later time points after WNV infection [**23**]. These results demonstrate that the RLR signaling pathway controls virus replication and induces innate immune responses against WNV infection in cortical neurons.

Neuronal destruction and CNS inflammation are enhanced in WNV infected IPS-$1^{-/-}$ mice

To determine the role of the RLR pathway in protection of neurons against WNV pathogenesis *in vivo*, we conducted histological analysis of brain tissue from wild type and IPS-$1^{-/-}$ mice infected with WN-TX (**Fig 4A**). Analysis of brain sections from infected wild type mice revealed little or no inflammation or

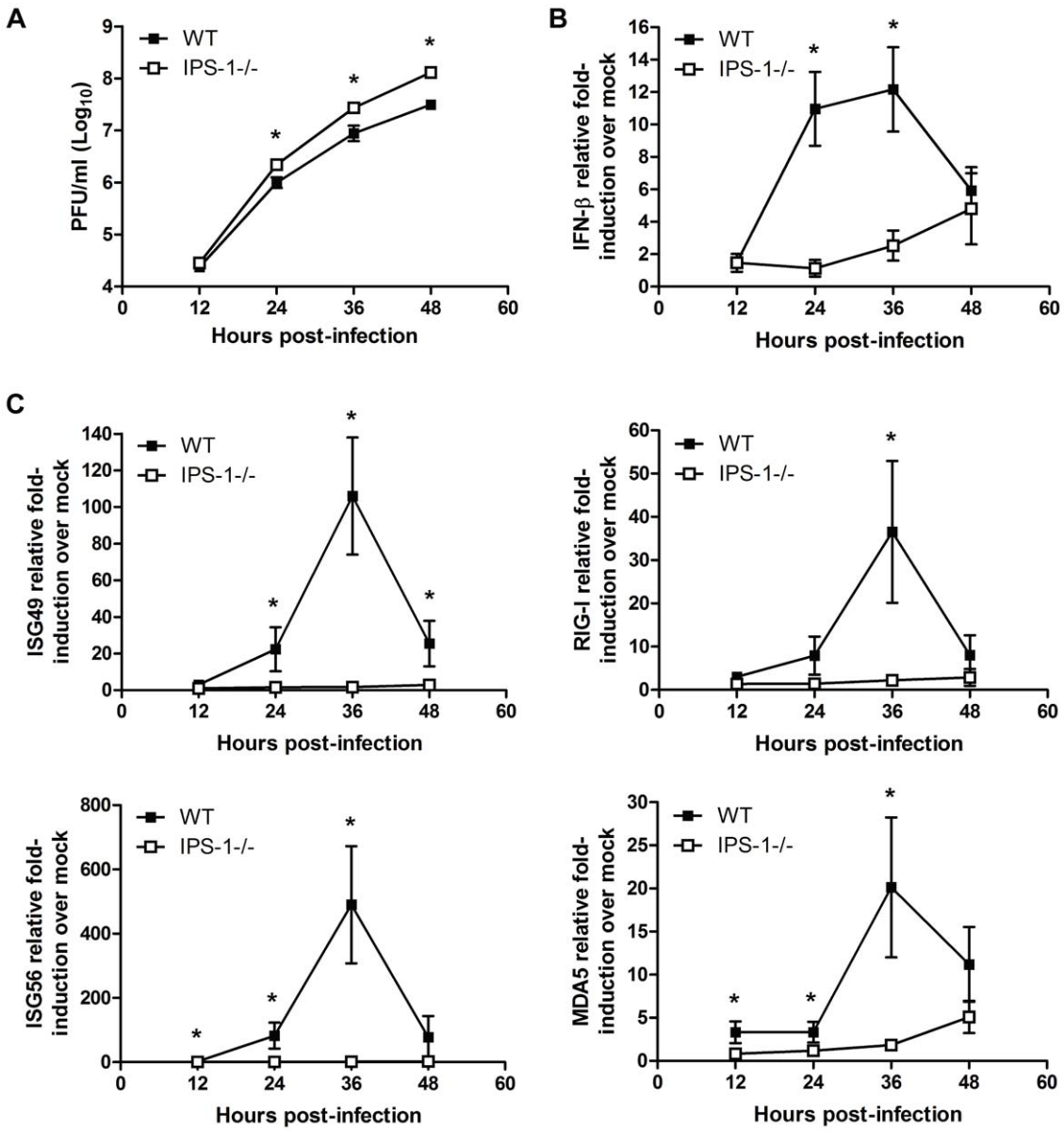

Figure 3. IPS-1 is essential for triggering innate immune defenses and controlling virus replication during WNV infection of primary cortical neurons. Primary cortical neurons (CN) from WT and IPS-$1^{-/-}$ mice were infected at an MOI of 1.0. (A) Viral titers in the culture supernatants were determined by plaque assay. (B, C) mRNA expression was determined by RT-qPCR assay using primers-specific for (B) IFN-β or (C) ISG56, ISG49, RIG-I, and MDA5. Graphs show the mean +/− standard deviation from triplicate independent analyses. Asterisks denote $p<0.05$.
doi:10.1371/journal.ppat.1000757.g003

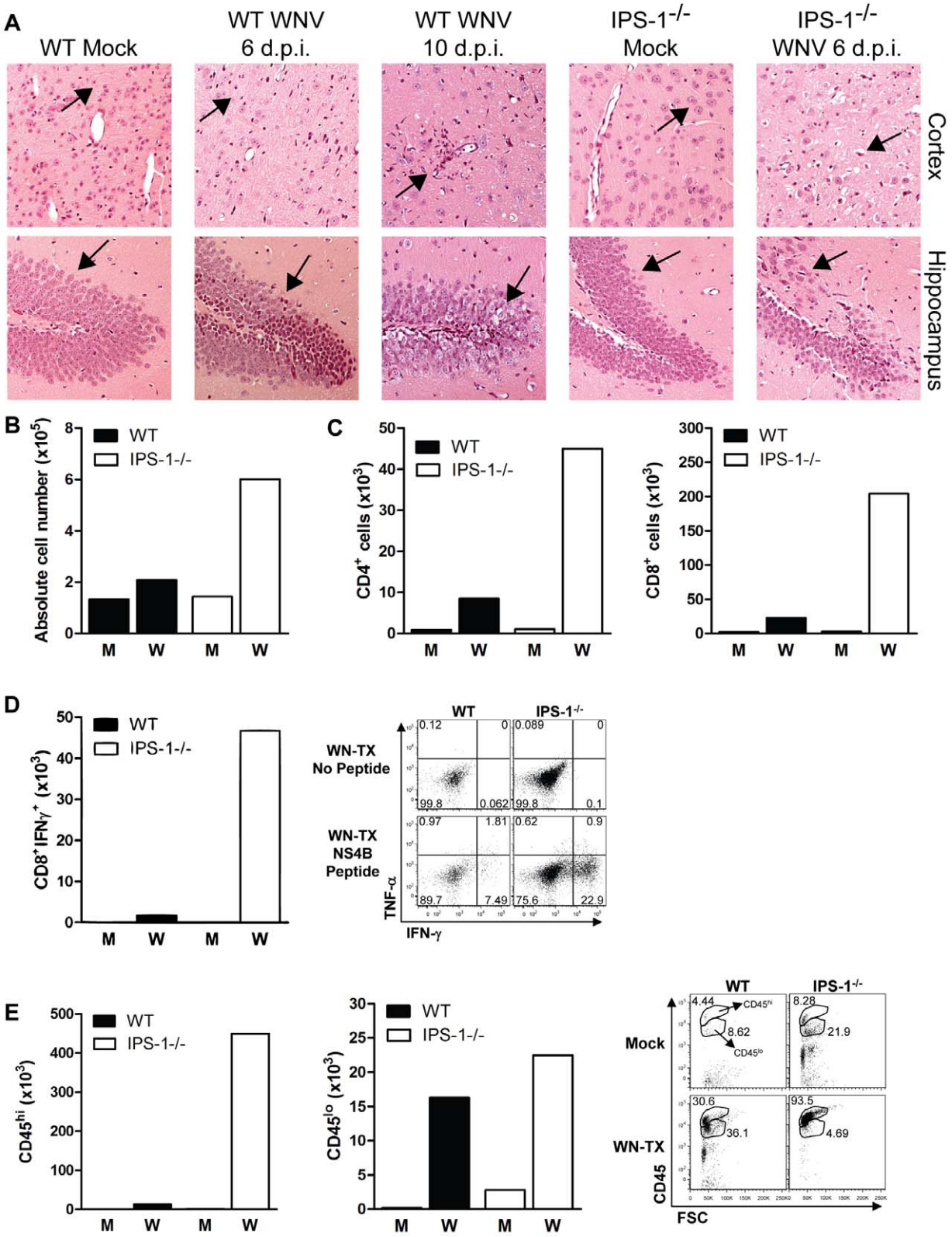

Figure 4. Increased CNS inflammation in WNV-infected IPS-1$^{-/-}$ mice. (A) H&E stained saggital brain tissue sections. The arrows denote areas of interest. (B–E) Brain leukocytes were recovered from wild type and IPS-1$^{-/-}$ mice six days pi. (B) The total number of brain lymphocytes was determined by cell counting. (C) Total CD4+ (left) and CD8+ T cells (right), (D) Total WNV-specific CD8+ T cells (left) with a representative analysis of the frequency of TNF-α and IFN-γ expression within brain CD8+ cells (right left), and (E) Total number of microglia/infiltrating macrophages (left) were determined by flow cytometry (right; representative analysis). M = Mock; W = WN-TX. Data are representative of two or more independent experiments, and each analysis represents a pool of 5 mouse brains.
doi:10.1371/journal.ppat.1000757.g004

neuronal damage, with sparse and focal cell infiltrates restricted to the hippocampus and cerebral cortex on day 6 pi. By day 10 pi (a timepoint in wild type mice in which peak virus replication in the CNS occurs [34]) cellular infiltrates were present in the parenchyma and neuronal destruction was observed throughout the cortex and hippocampus. In contrast, brain sections from infected IPS-$1^{-/-}$ mice recovered on day 6 pi displayed extensive injury to neurons in the cortex and granular neurons of the hippocampus. Damaged neurons appeared pyknotic with vacuolation, degeneration and cell dropout. Somewhat surprisingly, we observed extensive inflammation in the brains from infected IPS-$1^{-/-}$ mice within the cortex, hippocampus, and cerebellum (data not shown) displaying prominent perivascular and parenchymal immune cell infiltrates.

To evaluate the composition and antigen-specificity of the inflammatory cells within the brains of WNV-infected mice, lymphocytes were isolated from infected brains on day 6 pi and were characterized from pools (n = 5) of wild type and IPS-$1^{-/-}$ infected mice. Brains from IPS-$1^{-/-}$ infected mice showed an 2.9-fold increase in the total number of immune cells as compared to wild type infected mice (**Fig 4B**), and this was associated with an increase in absolute numbers of infiltrating CD4+ and CD8+ T cells (**Fig 4C**). Among the brain CD8+ T cells isolated from IPS-$1^{-/-}$ mice, there was a remarkable 27-fold increase in the number of antigen-specific cells that expressed IFN-γ after treatment with an immundominant NS4B peptide (**Fig 4D**) [35,36]. Analysis of microglia/Mϕ cells, based on relative surface expression of CD45 and CD11b [37], revealed increased numbers of microglial cells (CD45+^{lo}/CD11b+) and infiltrating macrophages (CD45+^{hi}/CD11b+) within the brains of infected IPS-$1^{-/-}$ mice when compared to wild type mice (**Fig 4E**). Similar findings were observed in the spinal cords from infected IPS-$1^{-/-}$ mice (data not shown). Combined with the histological analysis, these results demonstrate that in the absence of IPS-1, WNV infection induces a strong inflammatory response in the CNS. While this response is likely associated with increased viral loads, the failure of this increased inflammatory response to elicit protection or control CNS pathology, in the absence of IPS-1, suggests a role for the RLR signaling pathway as a regulatory program that controls the quality of the inflammatory response to WNV infection.

Serum cytokine levels

To further characterize how IPS-1 modulates the inflammatory response to WNV infection, we measured levels of systemic type I IFN, proinflammatory cytokines, and chemokines present in the serum of WNV-infected mice at 1 and 4 days pi. Paradoxically, a trend towards more rapid induction and increased levels of type I IFN were observed in the serum of IPS-$1^{-/-}$ mice compared to wild type mice (**Fig 5A**). We note that in this case type I IFN was detected and quantified through a mouse-specific type I IFN bioassay, which does not differentiate between the IFN-α or -β species. This result is consistent with our recent studies showing that serum type I IFN levels accumulate during WNV infection in an IRF-7-dependent but IRF-3-independent manner [8,9]. In this case IFN-α species are likely accumulating through a TLR7-dependent signaling pathway involving plasmacytoid DCs, which do not require the RLR pathway for IFN production [38]. More recently, Town et al. assessed the role of TLR7 and MyD88$^{-/-}$ during WNV infection and found that mice lacking MyD88 produced elevated levels of systemic IFN during WNV infection [25]. Thus, during WNV infection systemic IFN is regulated through RLR-dependent and independent processes. Correspondingly, when compared to wild type mice, IPS-$1^{-/-}$ infected animals, which show higher viremia (**Fig 1B**) produced increased serum levels of proinflammatory cytokines and chemokines in response to WNV infection. Elevated levels of systemic IL-6, TNF-α, CXCL10, and IFN-γ were observed at 1 and/or 4 days pi in IPS-$1^{-/-}$ mice (**Fig 5B**). Serum cytokine levels were also compared between uninfected wild type and IPS-$1^{-/-}$ mice and showed no differences in basal cytokine expression (data not shown). These results demonstrate that in the absence of IPS-1, greater proinflammatory cytokine and chemokine responses are induced during WNV infection.

Altered WNV-specific antibody profiles in IPS-$1^{-/-}$ mice

WNV-specific antibody responses are essential for suppressing viremia and virus dissemination and limiting lethal WNV infection [39,40]. To determine if a deficiency in IPS-1 modulated the quality and quantity of the humoral immune response, we characterized the antibody profile in sera during WNV infection. In wild type mice, neutralizing virus-specific IgM antibodies are typically detectable by day 4 pi with WNV and production of neutralizing virus-specific IgG antibodies follow between days 6 and 8 pi [40]. A time course analysis in wild type and IPS-$1^{-/-}$ infected mice showed that between 4 and 6 days pi, WNV-infected IPS-$1^{-/-}$ mice exhibited significantly higher levels of virus-specific IgM, IgG, and IgG subclasses as compared to infected wild type mice (**Table 1**). WNV-specific IgG1 antibodies were detected at low levels on day 6 pi in sera from wild type and IPS-$1^{-/-}$ mice. Additionally, we observed a ~72.9-fold increase in WNV-specific IgG2a levels in infected IPS-$1^{-/-}$ as compared to wild type mice on day 6 pi and ~2.2-fold increase on day 8 pi. Assessment of the virus-specific antibody responses through a PRNT assay revealed that neutralization titers in sera from wild type mice increased dramatically between 6 and 8 days pi. Sera from IPS-$1^{-/-}$ infected mice exhibited a modest increase in neutralization titer to 1:1280, despite having much higher levels of virus-specific antibodies. This difference translated into a serum neutralization index that was ~39-fold lower on day 6 pi in the infected IPS-$1^{-/-}$ mice compared to wild type mice. These results demonstrate that the humoral responses in WNV-infected IPS-$1^{-/-}$ mice are distinct from responses in wild type infected mice. Thus, RLR signaling and IPS-1 actions likely contribute to regulatory processes that govern the levels, IgG class switching, and neutralizing capacity of antibodies generated in response to WNV infection.

Enhanced inflammation in lymphoid organs associates with altered DC subsets and reduced numbers of regulatory T (T_{reg}) cells in WNV infected IPS-$1^{-/-}$ mice

To characterize the immune parameters associating with the dysregulated inflammatory and humoral responses in WNV infected IPS-$1^{-/-}$ mice, we analyzed the immune cell composition in draining lymph node and spleen tissues. Wild type and IPS-$1^{-/-}$ mice were challenged with diluent alone or with WN-TX, and draining popliteal lymph node (DLN) and the spleen were harvested at 1 and 6 days pi, respectively. Analysis of the popliteal DLN provides insight into how IPS-1 modulates the inflammatory response immediately after infection whereas assessment of the spleen elucidates characteristics of the adaptive immune response prior to the infection endpoint. Immune cells were isolated from the popliteal DLN and were characterized by flow cytometry (**Fig 6**). Analysis of CD8α DC subsets, which are phenotypically the major antigen presenting cells within lymphoid tissues and are implicated in eliciting virus-specific CD8 T cell in response to acute WNV infection [41], showed that infected wild type and IPS-$1^{-/-}$ mice exhibited similar increases in the

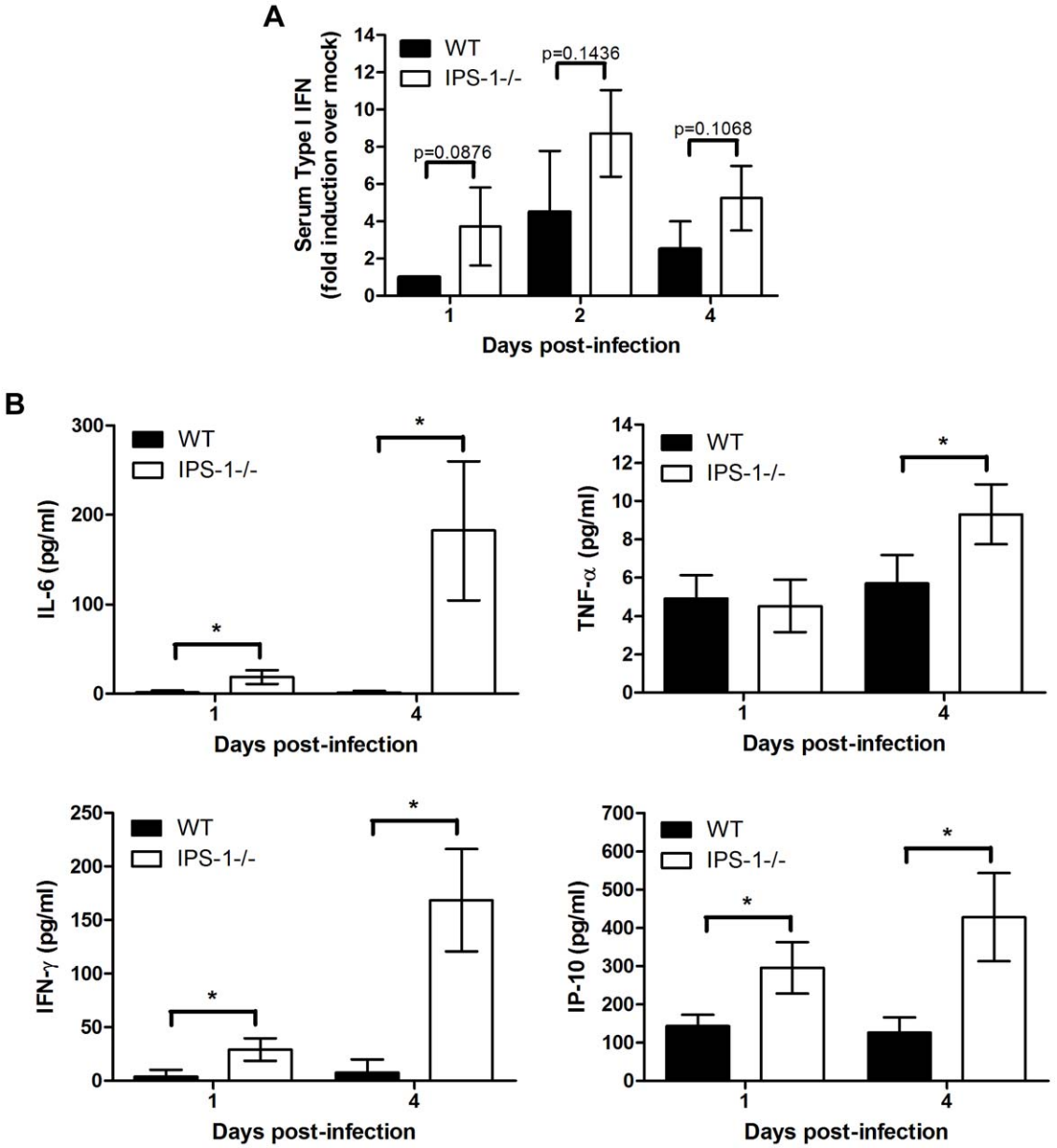

Figure 5. Enhanced levels of IFN, proinflammatory cytokines, and chemokines in serum from WNV-infected IPS-1$^{-/-}$ mice. Serum was collected from wild type and IPS-1$^{-/-}$ mice. (A) Type I IFN levels at 1, 2, and 4 days pi. (B) Proinflammatory cytokines and chemokines were measured on days 1 and 4 pi. Graphs show the mean +/− standard deviation from triplicate measurements of duplicate experiments. Asterisks denote $p<0.001$.
doi:10.1371/journal.ppat.1000757.g005

numbers of CD8α$^+$ and CD8α$^-$ DCs compared to mock-infected mice (**Fig 6A, B**). However, a significant increase (~3-fold; $p<0.05$) of a proinflammatory DC subset, characterized as CD11c$^+$CD11b^{hi}Ly6C$^+$, was observed within the popliteal DLNs of IPS-1$^{-/-}$ infected mice (**Fig 6C**). This DC subset is monocyte-derived and typically recruited to sites of acute inflammation where they propagate the inflammatory response [42]. We found that these DC subsets were not significantly expanded and showed no differences in their recruitment to the DLN in either wild type or IPS-1$^{-/-}$ infected mice at 12 hours pi (data now shown). Thus, as early as 24 hours pi, an elevated cellular inflammatory response is initiated in the IPS-1$^{-/-}$ mice. In contrast, similar increases in plasmacytoid DCs were observed within infected wild type and IPS-1$^{-/-}$ infected mice (**Fig 6D**), demonstrating that an absence of IPS-1 did not directly affect expansion and/or recruitment of this DC subset. Within the popliteal DLNs, mock-infected IPS-1$^{-/-}$ mice compared to wild type mice generally showed elevated numbers of B cells, CD4+ T cells ($p<0.05$), and CD8+ T cells (**Fig 6E, F, and G**). These results suggest that IPS-1 contributes to the homeostasis of lymphocyte populations within LNs. WNV infection of wild type mice increased the number of B cells (3.4 fold), CD4$^+$ T cells (3.1 fold), and CD8$^+$ T cells (2.3 fold; $p<0.05$) in the DLN within 24 hours pi. Similar increases in B cells were observed upon infection of IPS-1$^{-/-}$ mice. However, the number of CD4$^+$ and CD8$^+$ T cells was reduced in the DLN after WNV infection of IPS-1$^{-/-}$ mice. Thus, in the absence of

Table 1. WNV-specific antibody titers.

	Wild type			IPS-1$^{-/-}$	
	Day 4	Day 6	Day 8	Day 4	Day 6
IgM[a]	<20	160±49	1620±0	47±20	1620±0
IgG[b]	60±0	520±575	12150±4860	40±22	102060±45174
IgG1[b]	<20	20±0	<20	<20	20±0
IgG2a[b]	<20	126±203	4050±1620	<20	9180±6033
$PRNT_{50}$	<20	320±0	7040±3840	<20	1280±0
Neutralization Index[c]	<0.25	0.471	0.511	<0.23	.012

[a]IgM titers were determined by an arbitrary cutoff at an OD of 0.2 minus the value from mock infected mice.

[b]IgG, IgG1, and IgG2a titers determined by OD values that were greater than 3 standard deviations above background signal.

[c]Neutralization index was calculated by dividing $PRNT_{50}$ titers by the total IgM[a] plus IgG[b] titer for each point.

doi:10.1371/journal.ppat.1000757.t001

IPS-1, WNV infection specifically increases the number of inflammatory Ly6c$^+$ DCs but suppresses the overall expansion and/or recruitment of T cells in the DLN.

We further analyzed the lymphocyte composition of the spleen on day 6 after WNV infection (**Fig 7**). Gross pathologic analysis revealed that WNV infection of IPS-1$^{-/-}$ mice results in massive splenomegaly whereas infection of wild type mice induces only a slight increase in spleen size (**Fig 7A**). Cell analysis revealed increased numbers of total lymphocytes in the spleens of infected IPS-1$^{-/-}$ mice as compared to wild type mice (**Fig 7B**).

Regulatory T (T_{reg}) cells have recently been shown to contribute to the dampening of inflammation and adaptive immune responses during acute virus infections [26,43,44]. Moreover, a reduction in the number of circulating T_{reg} in mice leads to enhanced lethality after WNV infection [45]. A time course analysis of T_{regs} in wild type mice revealed that WNV infection results in a significant increase in the numbers of FoxP3+ T cells as compared to mock-infected mice beginning on day 4 and peaking by day 6 pi (**Fig 7C**), indicating the expansion of T_{regs} during acute WNV infection. Despite their marked increase in viral load, the infected IPS-1$^{-/-}$ mice did not display an increase in the numbers of FoxP3+ T cells at any timepoint analyzed. Thus, IPS-1 signaling directly or indirectly impacts T_{reg} proliferation and does so independently of viral load.

We also observed that spleens from infected IPS-1$^{-/-}$ mice exhibited significantly increased numbers of CD8+ T cells in comparison to those from infected wild type mice, whereas the expansion of splenic CD4+ T cells in wild type and IPS-1$^{-/-}$ mice were not different (**Fig 7D**). The spleens from WNV-infected IPS-1$^{-/-}$ mice showed significantly higher numbers (3.9-fold; $p<0.05$) of WNV-specific CD8+ T cells producing IFNγ.

To further define the phenotype associated with WNV-induced splenomegaly in IPS-1$^{-/-}$ mice, we also assessed the numbers of NK cells and neutrophils. Spleens from infected IPS-1$^{-/-}$ mice contained greater numbers of NK cells (CD4$^-$ CD8$^-$NK1.1$^+$cells), NKT cells (CD4+/CD8+/NK1.1+ cells) and neutrophils (CD11b$^+$Gr1$^+$ cells) (**Fig 7E**). Although WNV-infected wild type mice infected displayed slight increases in the absolute numbers of these specific cell types, a deficiency of IPS-1 resulted in a more marked enhancement of these immune cell populations.

Discussion

In this study, we establish a major role for RLR signaling in protection from WNV pathogenesis, and demonstrate that IPS-1 is critical for the control of WNV infection *in vivo*. Our studies indicate that IPS-1-dependent RLR signaling functions to establish balanced, effective, and protective innate and adaptive immune responses, and that IPS-1 links adaptive immune regulation with the innate immunity triggered by RLR signaling during WNV infection. In the absence of IPS-1 *in vitro*, innate immune defense programs of myeloid DCs and macrophages were ablated or severely attenuated. Moreover, *in vivo* analysis of infected IPS-1$^{-/-}$ mice showed altered IgG and IgM antibody responses with diminished virus neutralization activity. The inflammatory response to WNV infection is regulated by IPS-1-dependent processes such that a deficiency of IPS-1 resulted in elevated proinflammatory cytokine and chemokines and increased numbers of inflammatory DCs, antigen-specific T cells, natural killer cells, and neutrophils in lymphoid organs, and activated macrophage/microglial cells within the CNS. The dysregulated inflammatory response to WNV infection in IPS-1$^{-/-}$ mice was associated with a reduction in the numbers of T_{reg} cells and their failure to expand during acute infection. These observations demonstrate the critical role of IPS-1 in mediating RLR signaling of innate antiviral immunity against WNV infection, and reveal novel features of IPS-1 function in regulating immune homeostasis, inflammation, and adaptive immunity to infection.

Although infection of primary DCs, macrophages, and neuronal cells failed to induce type I IFN upon WNV infection, WNV-infected IPS-1$^{-/-}$ mice showed enhanced systemic type I IFN responses. This finding agrees with previous studies that indicate both IPS-1-dependent and -independent pathways contribute to the systemic type I IFN production *in vivo* [8,9,23,25]. Most importantly, the enhanced tissue tropism and rapid viral entry into the CNS observed in the IPS-1$^{-/-}$ mice is not affected by the elevated systemic IFN responses. This suggests that local tissue-specific and intracellular responses triggered by RLR-dependent signaling are more essential for reducing viral burden and dissemination. One possible explanation is that a distinct set of RLR-responsive genes function to control virus replication at the site of infection. This could explain, in part, the elevated levels of virus replication, enhanced tissue tropism and cell-to-cell spread in mice or cells deficient in IRF3 or IRF-7, each of which are downstream transcription factors of RLR signaling [8,9,10]. Additionally, it is likely that pDCs, which are specialized dendritic cells for producing systemic type I IFN during a viral infection [46], are likely contributing to the IFN responses observed during WNV infection. Studies by Silva et al. have shown that WNV triggers IFN induction in pDCs through a replication-independent manner [47]. Interestingly, within the DLN, we observed similar expansion of pDCs between wild type and IPS-1$^{-/-}$ infected mice, yet at the same timepoint (24 hours pi), elevated systemic type I IFN responses were observed in IPS-1$^{-/-}$ mice. This suggests two possibilities: 1) splenic pDCs or circulating pDCs are likely responding to the high levels virus in the serum from the IPS-1$^{-/-}$ infected mice to produce IFN at 24 hours pi and/or 2) various other cell types that express TLR3 and/or TLR7 are responding to WNV infection and contributing to systemic IFN responses. Taken together, these studies indicate that RLR signaling and the actions of IRF-3/7 are important in triggering IFN production and ISG expression to limit WNV replication and spread, and that TLR signaling may impart additional, RLR-independent defenses that regulate immunity against WNV infection.

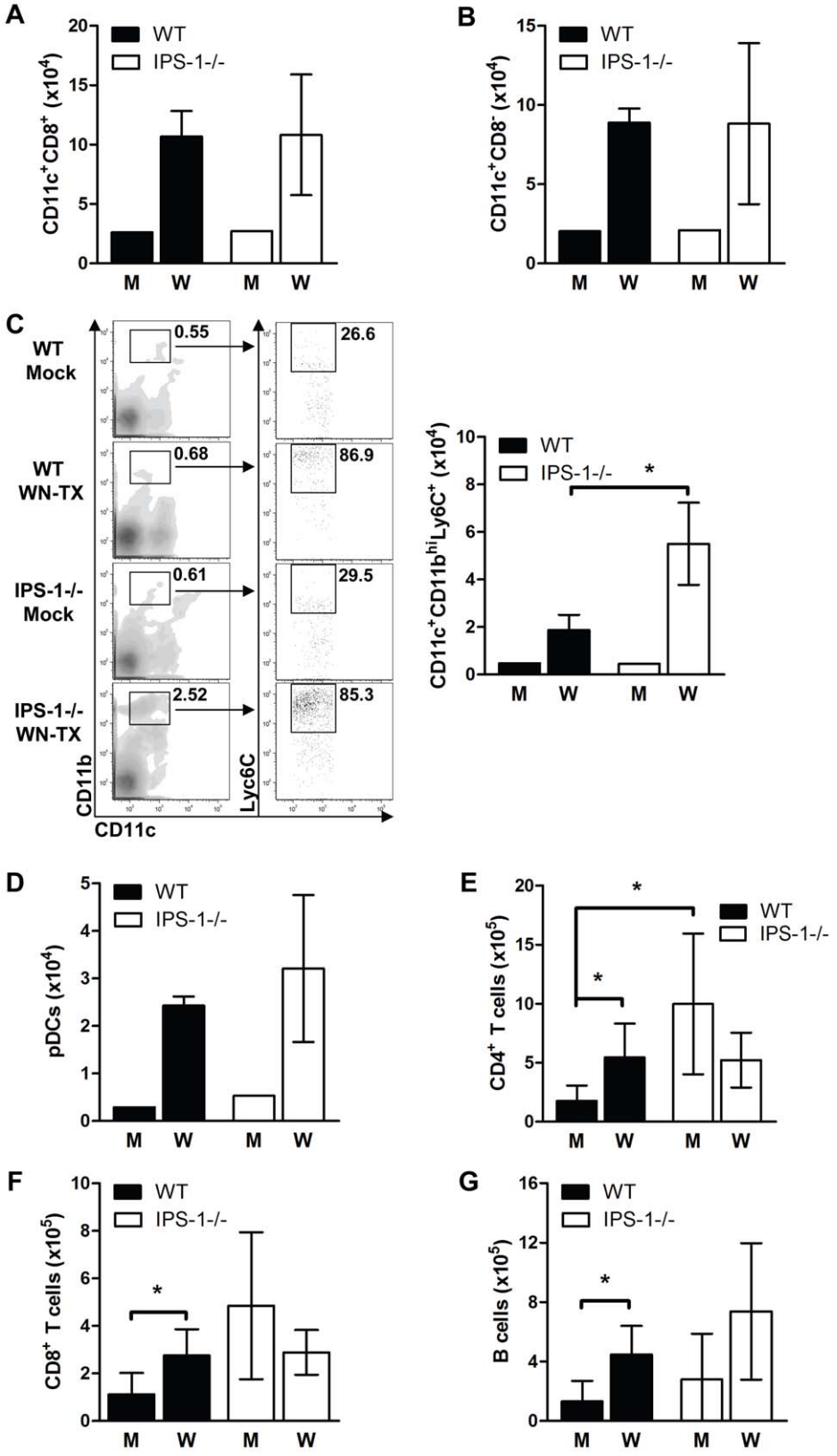

Figure 6. Immune cell subsets within the popliteal draining lymph node during acute WNV infection. Wild type and IPS-1$^{-/-}$ mice were mock-infected (M) or infected with WN-TX (W), and popliteal draining lymph nodes were harvested 24 hr later. Lymphoid cells were isolated and cells were analyzed by flow cytometry. (A–C) total numbers of cells expressing various dendritic cell surface markers, (D) plasmacytoid cell surface markers (CD11c$^{int/lo}$/B220+/siglec H+). (E and F) T cells (G) B cells. A representative flow cytometric analysis of the CD11c+/CD11b^{hi}/Ly6C+ DC subset is shown in C (left panel set). Data show the mean +/− standard deviation from triplicate samples of duplicate experiments. Asterisks denote $p<0.05$.
doi:10.1371/journal.ppat.1000757.g006

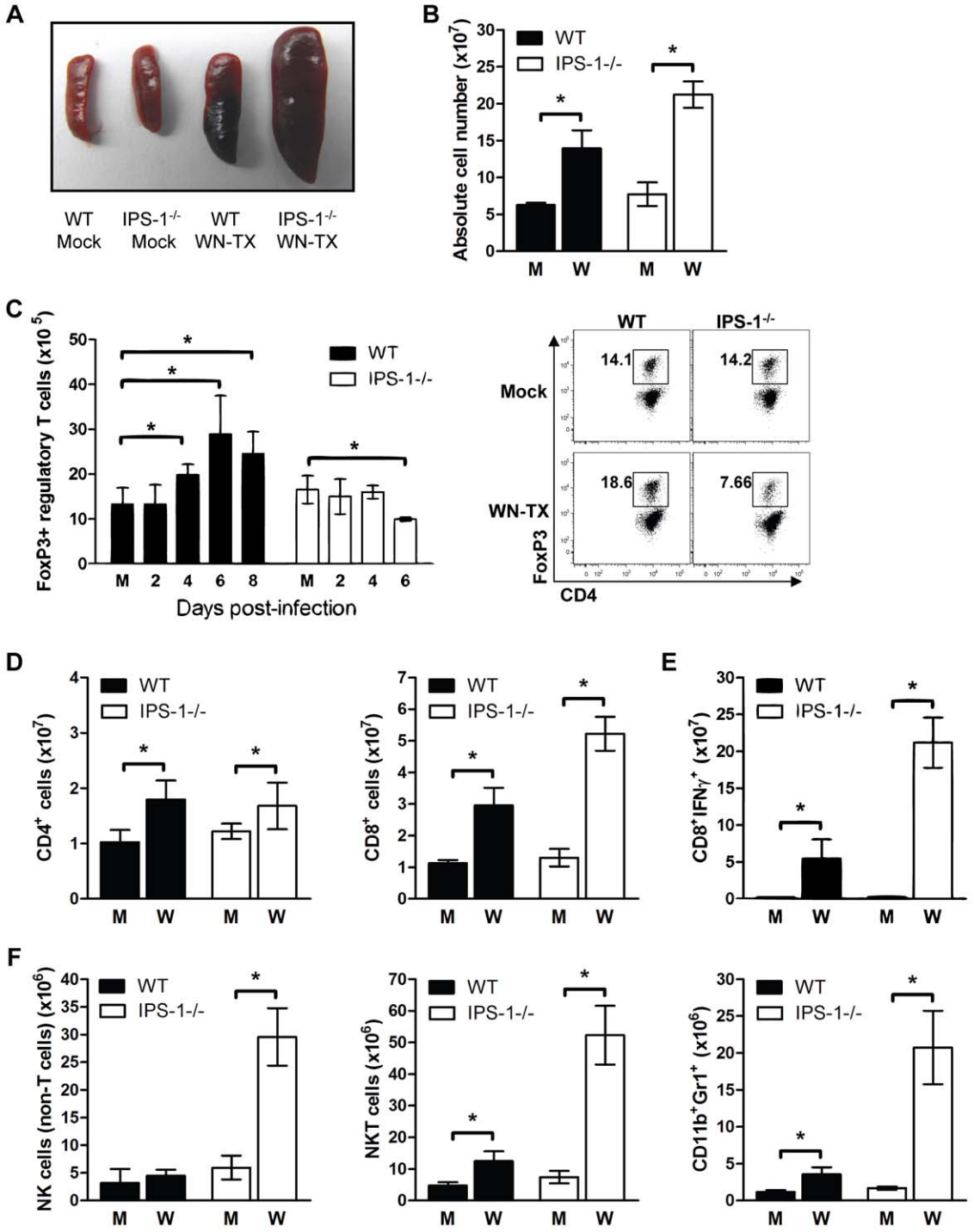

Figure 7. Enhanced inflammation in IPS-1$^{-/-}$ infected mice associates with a lack of T_{reg} expansion during WNV infection. Wild type and IPS-1$^{-/-}$ mice were mock-infected (M) or infected with WN-TX (W). Spleens were harvested and immune cells were isolated, counted, and characterized by flow cytometry. (A) Spleen morphology. (B) Absolute cell counts. (C) Total CD4+/FoxP3+ regulatory T cells (left; M = mock) and representative flow cytometric analysis of cell frequency from samples on day 6 pi (right). (D) CD4+ and CD8+ T cells. (E) NS4B antigen-specific CD8+ T cells. (F) CD4−/CD8−/NK1.1+ NK cells, CD4+/CD8+/NK1.1+ NKT cells, and CD11c+/Gr1+ neutrophils. Graphs show the mean +/− standard deviation from triplicate samples of duplicate experiments. Asterisks denote $p<0.05$.
doi:10.1371/journal.ppat.1000757.g007

The production of and response to type-I IFN is a major linkage point between innate and adaptive immunity, as IFN-α and IFN-β sustain B cell activation and differentiation [48,49,50], expand antigen-specific CD8+ T cells [51,52], CD4+ T cells [53], and activation of NK cells [54]. One of the most intriguing aspects of this study was the global alteration of the immune response elicited in the IPS-1$^{-/-}$ mice, indicating that RLR signaling couples innate immunity with regulation of the adaptive immune response. Infection of IPS-1$^{-/-}$ mice exhibited increased IgM and IgG WNV-specific antibodies, enhanced WNV-specific CD8+T cell

response, and increased expansion of neutrophils, NK cells and NK-T cells. One trivial explanation for these differences is that there is an increased antigen load in the absence of IPS-1 and, as a result, enhanced virus-specific (e.g. CD8+ T cells, IgG and IgM antibodies) and nonspecific (e.g. Neutrophils, NK cells) responses. However, there are several key findings from this study that argue against these responses simply being attributed to higher antigen load: (1) In the absence of IPS-1, the CD4 and CD8 T cells, which are protective against WNV infection [34,35,36,55,56,57,58], were significantly enhanced in the peripheral and CNS compartments but failed protect against infection. One explanation for this observation is that the expansion and migration of CD4 and CD8 T cells to different tissues was itself uncontrolled, resulting in T cell-mediated pathology rather than T cell-mediated protection. (2) While the quantity of virus-specific IgM and IgG antibody responses were greatly enhanced in the absence of IPS-1, there was a marked reduction in antibody quality in terms of neutralization capacity. In contrast deficiencies in TLR3 or MyD88 (data not shown) did not alter virus-specific antibody responses and neutralization capacities. Collectively, these findings suggest that RLR-dependent signaling coordinates effective antibody responses during WNV infection through as yet undefined pathway. (3) While systemic IFN responses provide a link between innate and adaptive immune responses, our studies suggest that the PRR signaling pathways (RLR-dependent vs – independent) and levels of IFN production in combination with production other proinflammatory cytokines or chemokines regulate the quantity and quality of the immune response during virus infection. Thus, in the absence of IPS-1 signaling, infected conventional DCs or Mϕ, two integral cell types in establishing adaptive immunity, likely do not produce IFN or the normal array and level of proinflammatory cytokines/ chemokines. Instead, IFN and other mediators may be strictly produced by infected or bystander cells during WNV infection, occurring with altered kinetics and magnitude, through TLR-dependent pathways, such as TLR3 and/or TLR7 [23,25]. (4) In the absence of IPS-1, the enhanced expansion of Ly6C+ "inflammatory" DCs failed to limit early WNV replication and dissemination. This inflammatory DC subset migrates to sites of infection, secretes pro-inflammatory cytokines, and promotes CD8+ T cell expansion during a secondary virus infection, suggesting it sustains the effector T cell response [59]. Our data indicate that Ly6C+ DC recruitment and/or expansion is governed by IPS-1-dependent events of RLR signaling. Thus, the aberrant recruitment/expansion of these inflammatory DCs may contribute to immunopathogenesis and limit development of an effective immune response to control WNV virus infection. (5) The lack of T_{reg} expansion during WNV infection correlated with altered IFN levels, increased proinflammatory cytokines and chemokine levels, and an increased number and distribution of antigen-specific CD8+ T cells. These observations implicate an indirect or direct role for IPS-1 in regulating T_{reg} levels during WNV infection, and provide evidence that links a lack of T_{reg} expansion to immune dysregulation.

While their importance in autoimmunity is established [60], recent studies have implicated an integral role for T_{regs} in controlling inflammation and adaptive immune responses during acute virus infections [26,43,44]. During acute infection T_{regs} function to locally contain and control the immune response with the dual outcome of suppressing viral dissemination while decreasing the likelihood of immune-mediated pathology. In support of this model, infection studies with herpes simplex virus (HSV) and mouse hepatitis virus (MHV), two well established models of viral encephalitis, have demonstrated the importance of T_{regs} in limiting proinflammatory cytokine and chemokine responses to protect the CNS and enhance survival [26,43]. Recent work also implicates T_{regs} in the control of WNV pathogenesis, wherein peripheral expansion of T_{regs} was associated with asymptomatic infection among WNV-infected blood donors but reduced T_{reg} levels associated with WNV disease [45]. Furthermore, these studies revealed that the conditional depletion of T_{reg} cells in mice results in enhancement of WNV virulence and expansion of antigen-specific CD8 T cells. Interestingly, from our studies, type I IFN does not appear to be the major contributor to T_{reg} expansion during WNV infection, as T_{regs} failed to expand in the IPS-$1^{-/-}$ infected mice despite their elevated levels of systemic type IFN. These observations suggest that RLR signaling through IPS-1 provides essential signals that directly or indirectly impart the expansion of T_{regs} during WNV infection.

We propose that IPS-1 coordinates an innate/adaptive immune interface wherein IPS-1- signaling after RLR engagement regulates the quantity, quality, and balance of the subsequent immune response. The integrity of the innate/adaptive immune interface is central to the eliminating virus but also restricting immunopathogenesis and inflammation during infection. RLR signaling is essential for triggering the innate immune response to RNA viruses that cause human disease, including the influenza viruses, respiratory syncytial virus and other paramyxoviruses, picornaviruses, reoviruses, flaviviruses, and hepatitis C virus [14,19,22]. Thus, in addition to WNV, IPS-1-dependent RLR signaling will likely have a broad impact for the control of inflammation, immune response quality, and viral disease.

Methods

Cells and viruses

BHK21 and L929 cells were maintained in Dulbecco's modified Eagle medium (DMEM) supplemented with 10% fetal bovine serum (FBS), 2mM L-glutamine, 1 mM sodium pyruvate, antibiotic-antimycotic solution, and 1× nonessential amino acids (complete DMEM). WNV strain TX 2002-HC (WN-TX) was isolated by as previously described [11]. Working stocks of WN-TX were generated by a single round of amplification on Vero-E6 (ccl-81; ATCC) cells, and supernatants were collected, aliquoted, and stored at −80°C. Virus stocks were titered by a standard plaque assay on BHK21 cells as previously described [40].

Mouse experiments

IPS-$1^{-/-}$ (C57BL/6×129Sv/Ev) and their wild type littermate control mice have been published [38,61] and were obtained as a generous gift from Dr. S. Akira (Osaka University, Osaka, Japan). Mice were genotyped and bred under pathogen-free conditions in the animal facility at the University of Washington. Experiments were performed with approval from the University of Washington Institutional Animal Care and Use Committee. The methods for mice use and care were performed in accordance with the University of Washington Institutional Animal Care and Use Committee guidelines. Age-matched six to twelve week old mice were inoculated subcutaneously (s.c.) in the left rear footpad with 100 PFU of WN-TX in a 10 µl inoculum diluted in Hanks balanced salt solution (HBSS) supplemented with 1% heat-inactivated FBS. Mice were monitored daily for morbidity and mortality.

Viral tissue burden and quantification

For *in vivo* virus replication studies, infected mice were euthanized, bled, and perfused with 20 ml of phosphate-buffered saline (PBS). Whole brain, spinal cord, kidney, and spleen were

removed, weighed, homogenized in 500ul of PBS, and titered by plaque assay.

Primary cell isolation and infection

Bone-marrow derived DC and Mϕ were generated as described previously [9]. Briefly, bone marrow cells from wild type and congenic deficient mice were isolated and cultured for 7 days in either RPMI-1640 supplemented with granulocyte-macrophage-colony stimulating factor, and interleukin-4 (Peprotech) to generate myeloid DC or in DMEM supplemented with macrophage colony stimulating factor (Peprotech) to generate Mϕ. On day 7, DC or Mϕ were infected with WN-TX at an MOI of 1.0 and at 12, 24, 36, and 48 hours post-infection (hpi), supernatants were collected for titration of viral burden by plaque assay on BHK21 cells and levels of IFN-β (described below). Cells were collected in parallel for western blot analysis. Cortical neurons were isolated from 15-day-old embryonic mice and cultured as described previously [62]. On day 6 of culture, neurons were infected with WN-TX at an MOI of 1.0 and at 12, 24, 36, and 48 hpi, supernatants were collected for virus titration by plaque assay on BHK21 cells and cells were collected for RNA analysis by RT-qPCR (described below).

Western blot analysis

Cells were lysed in modified RIPA buffer (10mM Tris [pH 7.5], 150mM NaCl, 0.5% sodium deoxycholate, and 1% Triton X-100) supplemented with protease inhibitor cocktail (Sigma) and phosphatase inhibitor cocktail II (Calbiochem). Protein extracts (25 μg) were analyzed by immunoblotting as described previously [11]. The following primary antibodies were used to probe blots: mouse anti-WNV from the Center for Disease Control; rabbit anti-ISG56, rabbit anti-ISG54, rabbit anti-ISG49, kindly provided by Dr. G. Sen; mouse anti-PKR from Santa Cruz; rabbit anti-RIG-I and rabbit anti-MDA5 from IBL; mouse anti-tubulin from Sigma; and rabbit anti-STAT-1 from Cell signaling. Secondary antibodies included peroxidase-conjugated goat anti-rabbit, goat anti-mouse, donkey anti-rabbit, and donkey anti-mouse were from Jackson Immunoresearch.

RNA extraction and analysis

For analysis of viremia, serum was separated (BD Microtainer tube SST) and RNA was extracted as previously described [8]. WNV RNA copy number was measured by RT-quantitative PCR (RT-qPCR) as previously described [63]. For cultured cells, total RNA was extracted using the RNeasy kit (Qiagen), DNase treated (Ambion) and evaluated for ISG49, ISG56, IFN-β, RIG-I, and MDA5 RNA expression by one-step SYBR Green RT-qPCR. Specific primer sets for ISG-49, ISG-56, RIG-I, and IFN-β have been described previously [30,64]. Primer sets for MDA5 are: 5′-GTGGTCGAGCCAGAGCTGAT and 3′- TGTCTCATG-TTCGATAACTCCTGAA.

Interferon bioassay and ELISA

IFN-α and -β were measured in sera using a biological assay as previously described [65]. Briefly, L929 cells were seeded at 3×10^4 cells/well in a 96 well plate one day prior to the addition of interferon standards or experimental samples. Mouse sera (diluted 1:10 in L929 media) were treated with UV light for 20 minutes to eliminate residual virus. Duplicate sera samples were then added to the 96-well plates in two-fold dilutions along with a murine IFN-β standard. The following day, EMCV challenge virus was added to the cells in 50 μl/well at an MOI of 5.0. Twenty-four hours later, cytopathic effect was measured by a blinded scorer and IFN levels in the sera was calculated based on the IFN standard. IFN-β in cell culture supernatants was analyzed using mouse-specific ELISA kits from PBL Biomedical Laboratories according to the manufacturer's protocol.

WNV-specific antibody analysis

WNV-specific IgM, total IgG, IgG1, and IgG2a levels were determined by an ELISA using purified recombinant E protein as previously described [55]. The neutralization titer of serum antibody was determined by using a previously described plaque reduction neutralization assay [40]. Briefly, sera samples from mock or WN-TX infected mice were diluted in DMEM followed by incubation at 56°C for 30 minutes to inactivate virus and complement factors. Sera were further diluted in two-fold increments and incubated with 100 PFU of WN-TX at 37°C for 1 hour. Standard plaque assays were performed on BHK21 cells and the dilution at which 50% of plaques were neutralized was determined by comparing the number of plaques formed from WNV-infected sera samples to mock infected sera samples.

Cytokine/chemokine analysis

WNV infected sera were analyzed for the presence and levels of TNF-α, IFN-γ, CXCL10 (IP-10), and IL-6 by a mouse-specific cytokine/chemokine Milliplex ELISA (Millipore).

Histological analysis

Mock-infected or WNV-infected mice were exsanguinated and perfused with PBS, 4% paraformaldehyde, pH 7.3. Brains were embedded in paraffin and 10-μm sections were prepared and stained with hematoxylin and eosin (H&E) by the UW histology pathology laboratory. Sections were analyzed using a Nikon Eclipse E600 microscope (UW Keck microscope facility).

Flow cytometric analysis

Draining lymph nodes from mice were isolated and digested with collagenase (Roche) and type I DNase in serum-free RPMI media at 37°C for 40 minutes with mechanical disruption. Cells were then incubated with RPMI media containing 10% FBS with EDTA and HEPES for 10 minutes at room temperature, pelleted, and resuspended in PBS containing 2% FBS and 0.1% sodium azide (FACS Staining buffer). Splenocytes were isolated, washed, and re-suspended in RPMI 1640 containing 10% FBS before *in vitro* stimulation. Cells were washed twice before FACS staining. For isolation of CNS immune cells, mice were euthanized and perfused extensively with PBS to remove residual intravascular leukocytes. Brains and spinal cords from 5 mice per experimental group were isolated and pooled. Tissues were minced in RPMI media, triturated, and digested with Liberase (Roche) and type I DNase in serum-free RPMI media at 37°C for 45 min. Immune cells were isolated after gradient centrifugation from a 37/70% Percoll interface and washed twice with FACS staining buffer. Immune cells were stained with antibodies specific to CD11c, CD11b, B220, CD3, CD25, CD4, CD8, NK1.1, Gr-1, siglec H, and CD45 (all reagents from eBiosciences). Intracellular FoxP3 staining was performed as previously described [26]. Intracellular IFN-γ staining was performed on splenocytes and CNS immune cells as previous described [35,36]. Briefly, lymphocytes were stimulated with 1 μg/ml of the WNV NS4B peptide (SSVWNAT-TAI) for 4 h at 37°C. Cells were washed and stained for cell surface markers followed by permeabilization-fixation using the Cytofix-Cytoperm Kit (BD-PharMingen) and stained with a Pacific-Blue conjugated IFN-γ antibody (eBiosciences) at 4°C for 30 min, washed and analyzed by flow cytometry. Flow cytometry

was performed on a BD LSRII machine using BD FACSDiva software. Cell analysis was performed on FlowJo (v.8.7.2) software.

Statistical analysis

For *in vitro* studies and immune cell analysis an unpaired student T-test was used to determine statistical differences. For *in vivo* viral burden analysis, Mann-Whitney analysis was used to determine statistical differences. Kaplan-Meier survival curves were analyzed by the log-rank test. A p-value ≤ 0.05 was considered significant. All data were analyzed using Prism software (GraphPad Prism5).

Acknowledgments

We thank Kristy Szetter and Jessica Briley for technical help and Robert Immormino for generation of purified WNV E protein for ELISA.

Author Contributions

Conceived and designed the experiments: MSS JML MG. Performed the experiments: MSS DYM ST JML MSD. Analyzed the data: MSS DYM JML NZ SD AR MB EAC MK MSD MG. Contributed reagents/materials/analysis tools: JML NZ SD AR MB EAC MK. Wrote the paper: MSS MG.

References

1. Cdc (2008) West Nile virus activity–United States, 2007. MMWR 57: 720–723.
2. Samuel MA, Diamond MS (2006) Pathogensis of West NIle virus infection: a balance between virulence, innate and adaptive immunity, and viral evasion. J Virol 80: 9349–9360.
3. Hayes EB, Sejvar J, Zaki S, Lanciotti R, Bode A, et al. (2005) Virology, pathology, and clinical manifestations of West Nile Virus disease. Emerg Infect Dis 11: 1174–1296.
4. Debiasi RL, Parsons JA, Grabert BE (2005) West Nile virus meningoencephalitis in an immunocompetent adolescent. Pediatr Neurol 33: 217–219.
5. Emig M, Apple DJ (2004) Severe West Nile virus disease in healthy adults. Clin Infec Dis 38: 289–292.
6. Fischer SA (2008) Emerging viruses in transplantation: there is more to infection after transplant than CMV and EBV. Transplantation 86: 1327–1339.
7. Suthar MS, Gale M Jr, Owen DM (2009) Evasion and disruption of innate immune signalling by hepatitis C and West Nile viruses. Cell Microbiol 11: 880–888.
8. Daffis S, Samuel MA, Keller BC, Gale M Jr, Diamond MS (2007) Cell-specific IRF-3 responses protect against West Nile virus infection by interferon-dependent and -independent mechanisms. PLoS Pathog 3: e106. doi:10.1371/journal.ppat.0030106.
9. Daffis S, Samuel MA, Suthar MS, Keller BC, Gale M Jr, et al. (2008) Interferon regulatory factor IRF-7 induces the antiviral alpha interferon response and protects against lethal West Nile virus infection. J Virol 82: 8465–8475.
10. Fredericksen BL, Smith M, Katze MG, Shi PY, Gale M Jr (2004) The host response to West Nile Virus infection limits viral spread through the activation of the interferon regulatory factor 3 pathway. J Virol 78: 7737–7747.
11. Keller BC, Fredericksen BL, Samuel MA, Mock RE, Mason PW, et al. (2006) Resistance to alpha/beta interferon is a determinant of west nile virus replication fitness and virulence. J Virol 80: 9424–9434.
12. Samuel MA, Diamond MS (2005) Alpha/beta interferon protects against lethal West Nile virus infection by restricting cellular tropism and enhancing neuronal survival. J Virol 79: 13350–13361.
13. Kang DC, Gopalkrishnan RV, Wu Q, Jankowsky E, Pyle AM, et al. (2002) mda-5: An interferon-inducible putative RNA helicase with double-stranded RNA-dependent ATPase activity and melanoma growth-suppressive properties. PNAS 99: 637–642.
14. Sumpter R, Loo YM, Foy E, li K, Yoneyama M, et al. (2005) Regulating intracellular anti-viral defense and permissiveness to hepatitis C virus RNA replication through a cellular RNA helicase, RIG-I. J Virol 79: 2689–2699.
15. Yoneyama M, Kikuchi M, Natsukawa T, Shinobu N, Imaizumi T, et al. (2004) The RNA helicase RIG-I has an essential function in double-stranded RNA-induced innate antiviral responses. Nat Immunol 5: 730–737.
16. Yoneyama M, Kikuchi M, Matsumoto K, Imaizumi T, Miyagishi M, et al. (2005) Shared and unique functions of the DExD/H-box helicases RIG-I, MDA5, and LGP2 in antiviral innate immunity. J Immunol 175: 2851–2858.
17. Kato H, Takeuchi O, Mikamo-Satoh E, Hirai R, Kawai T, et al. (2008) Length-dependent recognition of double-stranded ribonucleic acids by retinoic acid-inducible gene-I and melanoma differentiation-associated gene 5. J Exp Med 205: 1601–1610.
18. Saito T, Hirai R, Loo YM, Owen D, Johnson CL, et al. (2007) Regulation of innate antiviral defenses through a shared repressor domain in RIG-I and LGP2. PNAS 104: 582–587.
19. Loo YM, Fornek J, Crochet N, Bajwa G, Perwitasari O, et al. (2008) Distinct RIG-I and MDA5 signaling by RNA viruses in innate immunity. J Virol 82: 335–345.
20. Fredericksen BL, Gale M Jr (2006) West Nile virus evades activation of interferon regulatory factor 3 through RIG-I-dependent and -independent pathways without antagonizing host defense signaling. J Virol 80: 2913–2923.
21. Fredericksen BL, Keller BC, Fornek J, Katze MG, Gale M Jr (2008) Establishment and maintenance of the innate antiviral response to West Nile virus involves both RIG-I and MDA5 signaling through IPS-1. J Virol 82: 609–616.
22. Kato H, Takeuchi O, Sato S, Yoneyama M, Yamamoto M, et al. (2006) Differential roles of MDA5 and RIG-I helicases in the recognition of RNA viruses. Nature 441: 101–105.
23. Daffis S, Samuel MA, Suthar MS, Gale M Jr, Diamond MS (2008) Toll-like receptor 3 has a protective role against West Nile virus infection. J Virol 82: 10349–10358.
24. Wang T, Town T, Alexopoulou L, Anderson JF, Fikrig E, et al. (2004) Toll-like receptor 3 mediates West Nile virus entry into the brain causing lethal encephalitis. Nat Med 10: 1366–1373.
25. Town T, Bai F, Wang T, Kaplan AT, Qian F, et al. (2009) Toll-like receptor 7 mitigates lethal West Nile encephalitis via interleukin 23-dependent immune cell infiltration and homing. Immunity 30: 242–253.
26. Lund JM, Hsing L, Pham TT, Rudensky AY (2008) Coordination of early protective immunity to viral infection by regulatory T cells. Science 320: 1220–1224.
27. Belkaid Y, Rouse BT (2005) Natural regulatory T cells in infectious disease. Nat Immunol 6: 353–360.
28. Leon B, Ardavin C (2008) Monocyte-derived dendritic cells in innate and adaptive immunity. Immunol Cell Biol 86: 320–324.
29. Johnson CL, Gale M Jr (2006) CARD games between virus and host get a new player. Trends Immunol 27: 1–4.
30. Fensterl V, White CL, Yamashita M, Sen GC (2008) Novel characteristics of the function and induction of murine p56 family proteins. J Virol 82: 11045–11053.
31. Grandvaux N, Servant MJ, tenOever B, Sen GC, Balachandran S, et al. (2002) Transcriptional profiling of interferon regulatory factor 3 target genes: direct involvement in the regulation of interferon-stimulated genes. J Virol 76: 5532–5539.
32. Shrestha B, Gottlieb D, Diamond MS (2003) Infection and injury of neurons by West Nile encephalitis virus. J Virol 77: 13203–13213.
33. Xiao SY, Guzman H, Zhang H, Travassos da Rosa AP, Tesh RB (2001) West Nile virus infection in the golden hamster (Mesocricetus auratus): a model for West Nile encephalitis. Emerg Infect Dis 7: 714–721.
34. Shrestha B, Diamond MS (2004) Role of CD8+ T cells in control of West Nile virus infection. J Virol 78: 8312–8321.
35. Brien JD, Uhrlaub JL, Nikolich-Zugich J (2007) Protective capacity and epitope specificity of CD8(+) T cells responding to lethal West Nile virus infection. Eur J Immunol 37: 1855–1863.
36. Purtha WE, Myers N, Mitaksov V, Sitati E, Connolly J, et al. (2007) Antigen-specific cytotoxic T lymphocytes protect against lethal West Nile virus encephalitis. Eur J Immunol 37: 1845–1854.
37. Schafer A, Whitmore AC, Konopka JL, Johnston RE (2009) Replicon particles of venezuelan equine encephalitis virus as a reductionist murine model for encephalitis. J Virol 83: 4275–4286.
38. Kato H, Sato S, Yoneyama M, Yamamoto M, Uematsu S, et al. (2005) Cell type-specific involvement of RIG-I in antiviral response. Immunity 23: 19–28.
39. Diamond MS, Sitati EM, Friend LD, Higgs S, Shrestha B, et al. (2003) A critical role for induced IgM in the protection against West Nile virus infection. J Exp Med 198: 1853–1862.
40. Diamond MS, Shrestha B, Marri A, Mahan D, Engle M (2003) B cells and antibody play critical roles in the immediate defense of disseminated infection by West Nile encephalitis virus. J Virol 77: 2578–2586.
41. Hildner K, Edelson BT, Purtha WE, Diamond M, Matsushita H, et al. (2008) Batf3 deficiency reveals a critical role for CD8alpha+ dendritic cells in cytotoxic T cell immunity. Science 322: 1097–1100.
42. Lopez-Bravo M, Ardavin C (2008) In vivo induction of immune responses to pathogens by conventional dendritic cells. Immunity 29: 343–351.
43. Anghelina D, Zhao J, Trandem K, Perlman S (2009) Role of regulatory T cells in coronavirus-induced acute encephalitis. Virology 385: 358–367.
44. Ruckwardt TJ, Bonaparte KL, Nason MC, Graham BS (2009) Regulatory T cells promote early influx of CD8+ T cells in the lungs of respiratory syncytial virus-infected mice and diminish immunodominance disparities. J Virol 83: 3019–3028.
45. Lanteri MC, O'Brien KM, Purtha WE, Cameron MJ, Lund JM, et al. (2009) Tregs control the development of symptomatic West Nile virus infection in humans and mice. J Clin Invest 119: 3266–3277.
46. Asselin-Paturel C, Trinchieri G (2005) Production of type I interferons: plasmacytoid dendritic cells and beyond. J Exp Med 202: 461–465.
47. Silva MC, Guerrero-Plata A, Gilfoy FD, Garofalo RP, Mason PW (2007) Differential activation of human monocyte-derived and plasmacytoid dendritic

cells by West Nile virus generated in different host cells. J Virol 81: 13640–13648.
48. Purtha WE, Chachu KA, Virgin HW, Diamond MS (2008) Early B-cell activation after West Nile virus infection requires alpha/beta interferon but not antigen receptor signaling. J Virol 82: 10964–10974.
49. Coro ES, Chang WL, Baumgarth N (2006) Type I IFN receptor signals directly stimulate local B cells early following influenza virus infection. J Immunol 176: 4343–4351.
50. Fink K, Lang KS, Manjarrez-Orduno N, Junt T, Senn BM, et al. (2006) Early type I interferon-mediated signals on B cells specifically enhance antiviral humoral responses. Eur J Immunol 36: 2094–2105.
51. Kolumam GA, Thomas S, Thompson LJ, Sprent J, Murali-Krishna K (2005) Type I interferons act directly on CD8 T cells to allow clonal expansion and memory formation in response to viral infection. J Exp Med 202: 637–650.
52. Thompson LJ, Kolumam GA, Thomas S, Murali-Krishna K (2006) Innate Inflammatory Signals Induced by Various Pathogens Differentially Dictate the IFN-I Dependence of CD8 T Cells for Clonal Expansion and Memory Formation. J Immunol 177: 1746–1754.
53. Havenar-Daughton C, Kolumam GA, Murali-Krishna K (2006) Cutting Edge: The direct action of type I IFN on CD4 T cells is critical for sustaining clonal expansion in response to a viral but not a bacterial infection. J Immunol 176: 3315–3319.
54. Gerosa F, Gobbi A, Zorzi P, Burg S, Briere F, et al. (2005) The reciprocal interaction of NK cells with plasmacytoid or myeloid dendritic cells profoundly affects innate resistance functions. J Immunol 174: 727–734.
55. Shrestha B, Samuel MA, Diamond MS (2006) CD8+ T cells require perforin to clear West Nile virus from infected neurons. J Virol 80: 119–129.
56. Wang Y, Lobigs M, Lee E, Mullbacher A (2003) CD8+ T cells mediate recovery and immunopathology in West Nile virus encephalitis. J Virol 77: 13323–13334.
57. Brien JD, Uhrlaub JL, Nikolich-Zugich J (2008) West Nile virus-specific CD4 T cells exhibit direct antiviral cytokine secretion and cytotoxicity and are sufficient for antiviral protection. J Immunol 181: 8568–8575.
58. Sitati EM, Diamond MS (2006) CD4+ T-cell responses are required for clearance of West Nile virus from the central nervous system. J Virol 80: 12060–12069.
59. Wakim LM, Waithman J, Van Rooijen N, Heath WR, Carbone FR (2008) Dendritic cell-induced memory T cell activation in nonlymphoid tissues. Science 319: 198–202.
60. La Cava A (2008) Tregs are regulated by cytokines: implications for autoimmunity. Autoimmun Rev 8: 83–87.
61. Kumar H, Kawai T, Kato H, Sato S, Takahashi K, et al. (2006) Essential role of IPS-1 in innate immune responses against RNA viruses. J Exp Med 203: 1795–1803.
62. Samuel MA, Whitby K, Keller BC, Marri A, Barchet W, et al. (2006) PKR and RNase L contribute to protection against lethal West Nile Virus infection by controlling early viral spread in the periphery and replication in neurons. J Virol 80: 7009–7019.
63. Linke S, Ellerbrok H, Niedrig M, Nitsche A, Pauli G (2007) Detection of West Nile virus lineages 1 and 2 by real-time PCR. J Virol Met 146: 355–358.
64. Saito T, Owen DM, Jiang F, Marcotrigiano J, Gale M Jr (2008) Innate immunity induced by composition-dependent RIG-I recognition of hepatitis C virus RNA. Nature 454: 523–527.
65. Shabman RS, Morrison TE, Moore C, White L, Suthar MS, et al. (2007) Differential induction of type I interferon responses in myeloid dendritic cells by mosquito and mammalian-cell-derived alphaviruses. J Virol 81: 237–247.